CHALMERS

Lumped Parameter Thermal Modelling of Electric Machines

Analysis of an Interior Permanent Magnet Synchronous Machine for Vehicle Applications

Master of Science Thesis

BJÖRN ANDERSSON

Department of Energy and Environment
Division of Electric Power Engineering
CHALMERS UNIVERSITY OF TECHNOLOGY
Göteborg, Sweden, 2013

Abstract

Two thermal resistance network models have been developed for the steady state radial heat flow an experimental IPMSM. The models have been based on published material, but also on some case studies with the purpose of determining the best choice of methods for certain situations. In one case study on hollow cylinders, it is concluded that it is favourable to place nodes with heat sources representing evenly distributed losses in a point corresponding to the mean radius of the object, rather than the resistive midpoint. Furthermore it is investigated whether the accuracy of a thermal resistance network model can be improved by increasing the resolution of the node configuration. The result indicates that so is the case, although with some ambiguity. The increased complexity of the high resolution network makes it more bulky however, which is a disadvantage compared to the low resolution node configurations.

The two network models are used to analyse the IPMSM, and compared with a FEM model made in ANSYS Mechanical. A number of parameters are swept to investigate the machines dependency on some thermally important design characteristics, and also the sensitivity to errors from uncertain input data, geometry approximations, and other estimations. Such uncertain parameters are e.g. the interface gaps between machine components, the turbulence model in the air gap, and the thermal model of the slots. Regarding the design aspects, it is suggested to strive towards minimising the contact gaps during the assembly, and consider the choice of materials used in the stator slots.

Keywords: Thermal Modelling, PMSM, Electric Machines, Thermal Resistance Network, FEM

Acknowledgement

Contents

Symbols and Abbreviations

Symbols

A	Area
G	Thermal conductance
h	Thickness
J	Current density
L	Path length
l	Length
Nu	Nusselts number
n	Node
no	Number
P	Power
r	Radius
T	Temperature
Ta	Taylor's number
V	Volume
α	Heat transfer coefficient
η	Efficiency
γ	Ratio
κ	Thermal expansion coefficient
λ	Thermal Conductivity
ρ	Electrical resistivity, density
ϕ	Angle
Φ	Circumference
μ	Dynamic viscosity
ω	Angular speed
θ	Angle, temperature
$\boldsymbol{G}$	Thermal conductance matrix
$\boldsymbol{P}$	Loss vector
$\boldsymbol{\Theta}$	Temperature vector

Subscripts

Al	Aluminium
amb	Ambient
a	Axial
c	Core
C	Complex network circuit model
Cu	Copper
el	Electrical
Fe	Iron
f	Friction, frame
g	Air gap
i	Inner
m	Magnet
n	Nominal
o	Outer
per	peripheral
r	Rotor
S	Simple network circuit model
s	Slot
sh	Shaft
st	Stator
Sym	Symmetry
th	Thermal
w	Windings
wi	Windage
y	Yoke
$resMid$	Resistive midpoint
$radMid$	Radial midpoint
$volMid$	Volumetric midpoint

Abbreviations

CAD	Computer-Aided Design
CFD	Computational Fluid Dynamics
ECMA	Scripting standard
FEM	Finite Element Method
HSPMG	High Speed Permanent Magnet Generator
IHG	Internal Heat Generation
PHEV	Plug-in Hybrid Electric Vehicle
PMSM	Permanent Magnet Synchronous Machine
rpm	revolutions per minute
xEVCO	Crossing Electric and Vehicle Competences

1 Introduction

The usage of electric drive systems in vehicles has undergone a rapid increase of popularity for some time now and is here to stay. One area where efforts are being directed at technical improvements is the bridge between the electrical and the thermodynamic aspects of electric machines. There are potential benefits to draw from knowing more about the behaviour and the effects of the heat that is generated in the machine during operation. It is of great importance to make sure that its temperature does not reach levels above what is tolerable, especially for sensitive parts such as permanent magnets and winding insulation. For machines used in environments where cooling is an especially challenging task, which is the case for electric vehicles, this understanding is perhaps of even greater importance.

xEVCO, *Crossing Electrical and Vehicle Competences*, is a collaboration project including Volvo Cars, Chalmers University of Technology and SP. It was initiated 2010 with the intent of increasing the knowledge in hybrid vehicle technology through funding of a number of research projects. This thesis is a project associated with xEVCO, and although the results is largely general to PMSM motors (*Permanent Magnet Synchronous Machines*), it was investigated with machines applicable to electric vehicle use in mind.

1.1 Problem Description

The thermal limits set the constraints of the machine. Go beyond them and you will decrease the life time of the machine. Do not go near them, and some of the potential of the machine is wasted. If the thermal constraints can be taken into account at an early stage in the optimisation process of the machine design, it is possible to achieve a more homogenous temperature distribution and avoid hot spots in the machine. The information could be useful for improving the overall design in terms of efficiency, torque/power density, overload time capability [1, p.11], and requirements on the cooling. Having a good knowledge of the actual levels means being able to design without having to resort to unnecessary large safety margins, which are usually costly.

A number of existing publications describe different aspects of the thermal modelling of electric motors. On synchronous machines with interior magnets however, it has not been written much. Having a detailed model opens up for a lot of possible questions to be investigated. A closer investigation of the modelling of an IPMSM is of particular interest, as it is the type of electrical motor used in the new V60 Plug-in Hybrid Electric Vehicle (PHEV) presented recently by Volvo.

The models should be parametric, and the parameters swept within reason-

able intervals based on the uncertainty of and sensitivity to the parameter in question. From this data, the most relevant parameters should be identified, and thus criteria for thermal aspects of designing an electric drive can be formulated.

The model has been based on a PMSM machine situated at Chalmers, upon which thermal measurements will be carried out in the future. Since the model is parameterised, it is general enough to be applicable for investigating changes for a number of different motor designs.

1.2   Previous Work
1995 Gunnar Kylander presented a thesis presenting a thermal resistance network model for a fan-cooled, caged induction machine with 36 stator slots. Several later papers treating thermal modelling of different types of machines have been based on or referred to the the work of Kylander. These include a licentiate thesis by Joachim Lindström (1999) who modify Kylanders model for a water-cooled surface mounted PMSM machine with 48 stator slots, and Janne Nerg et al. who have published several papers on the subject. Other and more recent important contributions to the field have been made by Aldo Boglietti et al. who have focused more on the specific problematic aspects, such as contact resistances between different materials.

1.3   Purpose
The purpose of this thesis is to develop a lumped parametric thermal network model for a PMSM machine. The machine in question is one with a low number of stator slots and interior permanent magnets. In that regard it differs from the machines modelled in the majority of today existing publications, which might mean that conventional methods are not always the optimal. Since most of the heat flow taking place in a radial flux machine is in the radial direction, and the impact of the axial heat flux taking place is generally regarded as rather small, the network is limited to modelling radial and circumferential phenomena. For verification purposes a FEM-based model is developed in parallel using the ANSYS software suite.

The model should provide a means to answer questions regarding the thermal behaviour of electric motors. It should be investigated how the temperature in different parts of the machine is dependent of some important geometrical properties. From the analysis some conclusions can be drawn regarding which design parameters are critical for the temperature distribution, and where care should be taken due to uncertainties in the model.

1.4 Scope

The topic of thermal modelling and simulation of electric motors includes some rather extensive questions, that can not all be satisfactory answered within the time constraints of a single thesis. Two such are the accurate predictions of machines losses and the electromagnetic properties of the machine. These will not be investigated in detail.

1.5 Method

The model has been developed iteratively, starting out with a simplified model of low complexity and only the basic components. Accuracy and details were added as knowledge of which the key factors and challenges increased. Established methods have usually been examined first, and have some times been implemented straight from the source. Other times some new ideas have been tested with the intention of improving accuracy or simply adapting to better suit the motor in question.

In parallel with the development of the thermal network, the same thing is simulated in FEM software for the sake of checking the validity of the model. The results yielded for either should be consistent, and the redundancy of having two methods of calculating should give an indication to the reliability of the results.

Although the FEM solution has the potential of being very detailed and accurate, it is never more correct than the input data. If assumptions regarding e.g. materials, contact gaps, air properties etc. are not entirely correct, these errors will be reflected in the simulation output. Furthermore, the software used is limited to treating all fluids as solids, meaning that the same methods for modelling convection in the air gap will be adapted for the FEM simulation. In other words, the FEM simulation is not intended to be interpreted as the absolute truth, but rather to give some idea of the veracity of the calculations.

1.5.1 Simulation Setup

It is important to make sure that both ways of modelling consistently investigates the same machine at the same operation point. It has therefore been of high priority to make sure configurations are easily accessible and to as large extent as possible gathered at a single place. This affects usability, but more importantly it lowers the risk of inadvertently comparing the results from different models when different settings have been used.

The thermal resistance network modelling is written in the programming language Python. The program is modular in the sense that different sets of parameters can be loaded and run in parallel by including different configuration files. General settings and the structure of the program, such as parameter sweeping and temperature iteration functionality, are done in the

main-file. The output is presented as a set of log files containing the values of the most relevant machine parameters and the resulting temperatures. The function of the program is presented in a flowchart in figure 1.

The FEM-simulations are done in the multiphysics software suite provided by ANSYS. It includes tools for a large number of problems and situations, of which mainly three programs have been of use:

ANSYS Maxwell is a program commonly used for simulations of electromagnetic fields. For this thesis however, the usage of Maxwell have mainly consisted of CAD work. The reason for choosing this over other available and compatible CAD software is mostly familiarity, but also the relative ease for scripting to update the geometry, and to have the option of later adding electromagnetic simulations.

ANSYS Mechanical offers a range of functionalities related to structural dynamics. Among them are thermal calculations.

ANSYS Workbench bridges the different programs in the software suite. Through it, the different components and systems can communicate with each other and share common variables, models and solutions.

A high number of simulations will be run and so altering the simulation model must be automated to a large extent. The most sensible way to achieve this is through scripting. Currently, Maxwell can be commanded through a scripting language based on the *ECMA* scripting standard. Changing things in Mechanical requires a combination of Javascript and the native APDL language. When incorporating these in the same simulation however, scripting commands can not be sent directly to either. Then they must go through Workbench, which in turn only responds to Workbench Journalling, yet another scripting language which is based on the Python syntax.

The interfacing of the thermal network simulation program and the FEM-simulation is done by generating a Workbench script for the same setup every time a network simulation is made. The script inherits all relevant parameters such as machine geometry, ambient temperature, materials and material properties, which parameter is to be swept etc. The results from the network simulation so that it can be presented together in a final log file after the simulation in ANSYS has been performed.
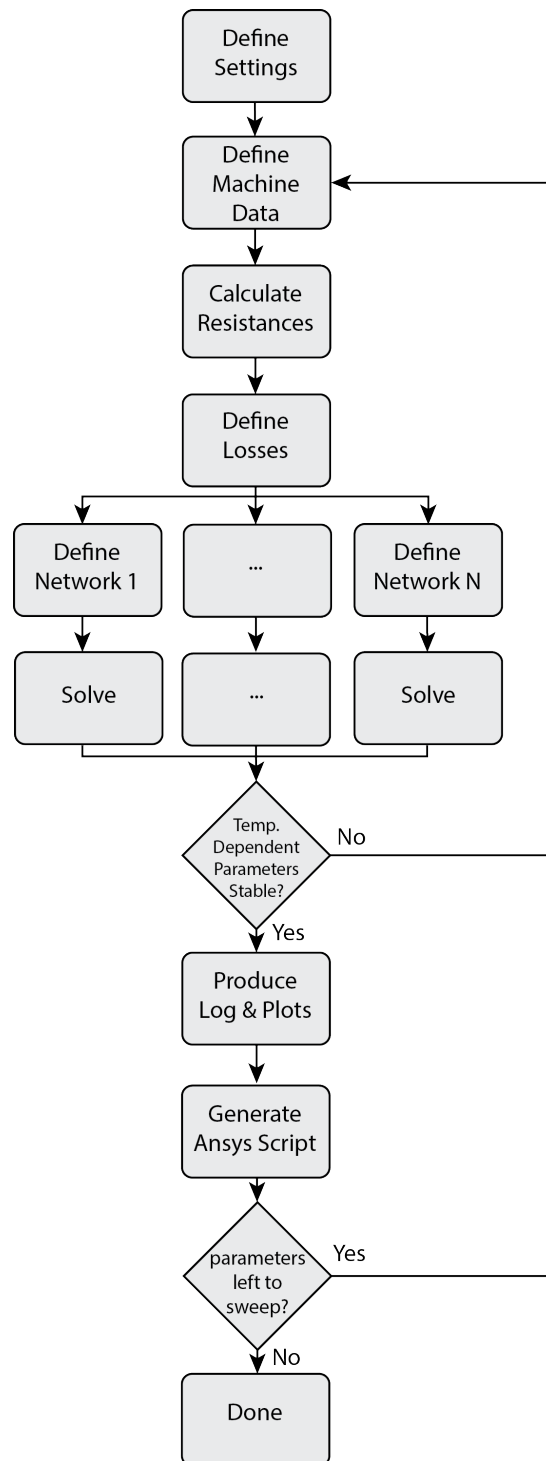
Figure 1: The structure of the program solving the thermal resistance network models.

2 Thermal Modelling Background

Thermal modelling is about describing the thermal behaviour of a system using mathematical means. It allows one to answer questions of how heat will be distributed depending on material properties and geometries, and how the system will react to changes in input.

To the benefit of those with a basic understanding of electronics, thermal systems are said to be analogous with electric circuits [2, p.2]. That means that the equations and boundary conditions governing the behaviour of one of the systems can be used to describe another by simply replacing the symbols of the variables, and the basic laws of electric circuits all apply for a corresponding thermal network. The relations between some important quantities are shown in Table 1.

As the use of thermal quantities will be very frequent and repetitive throughout this report, the subscript *th* will henceforth be dropped of the symbols, and e.g. a single R in an equation will always refer to the thermal quantity.

Table 1: The relation between some electric and thermal quantities

Electrical Quantities			Thermal Quantities		
Potential	V	$[V]$	Temperature	θ	$[^{\circ}K]$
Current	I	$[A]$	Heat	Q	$[W]$
Current density	J	$[A/m^2]$	Heat flux	q	$[W/m^2]$
Conductance	G_{el}	$[S]$	Thermal conductance	G_{th}	$[W/K]$
Conductivity	σ_{el}	$[S/m]$	Thermal conductivity	λ	$[W/mK]$
Resistance	R_{el}	$[\Omega]$	Absolute Thermal resistance	R_{th}	$[K/W]$
Resistivity	ρ	$[\Omega/m]$	Thermal resistivity	ρ_{th}	$[mK/W]$
Capacitance	C_{el}	$[F]$	Thermal capacitance	C_{th}	$[J/^{\circ}K]$

2.1 Heat Transfer Mechanisms

The second law of thermodynamics tells us that there is always net entropy increase in real processes. Entropy which is often described as the measure of disorder in a system, can also be used to describe the quality of the energy in a system. Low quality means a high level of disorder, and the highest possible entropy would be having the energy evenly distributed in space. Therefore, the second law of thermodynamics could also be explained by saying that an isolated system always strives for thermal equilibrium. Or, even more simply put, heat will flow from a hot place to a cooler place [3].

There are essentially three processes through which the transfer of heat can occur. *Conduction* is the transmission of energy between molecules in a medium. Although it is the only mechanism that takes place in solids, it is not exclusive to it, but takes place in fluids as well. The process is linear

and can be described by

$$P = G(T_i - T_j) \tag{1}$$

where P is the power flow, G is the thermal conductance, and T_i and T_j are the temperatures in two adjacent nodes.

In fluids and gases you also find the phenomena of *convection*. As the molecules in a non-solid medium are free to move around, the heat transfer ability of the medium is improved by the transportation of the molecules themselves, intermixing molecules of different energy levels and increasing the rate by which they come in contact with others. Just as for pure conduction, the mechanism is linear and can be described by (1).

The third process is that of *radiation*, which describes the mechanism of a body emitting photons carrying energy. The amount of radiation a body emits depends on the emissivity of the object, the surface area, but more strongly also the temperature [4]. The net energy transfer can be described by

$$P = G(T_i{}^4 - T_j{}^4) \tag{2}$$

In an electric machine, convection and radiation will contribute to the air gap and the frame-ambient thermal conductance. The effects of radiation tends to be rather small for electric machines [5], and will therefore be neglected. Furthermore, the process of predicting the motion of fluids can be very complicated and time consuming. This report will not go into details on the modelling of air, and instead make use of existing methods provided by Kylander and Lindström. In that way the complexity can be kept down and more focus kept on the geometry.

2.1.1 Thermal Resistance of Solids

Unlike properties such as *mass* or *conductivity*, thermal resistance of an object is calculated in respect to the direction of the heat flow [1, p. 44].

The thermal conductance across a homogenous object can be calculated by

$$G = \frac{\lambda A}{L} \tag{3}$$

where λ is the thermal conductivity, A the cross sectional area, and L the distance between the nodes. Accordingly, the thermal resistance is

$$R = \frac{1}{G} = \frac{L}{\lambda A} \tag{4}$$

Allowing the area of the conductor to vary over L results in the integral

$$R = \int_0^L \frac{1}{\lambda A(l_{path})} \mathrm{d}l_{path} \tag{5}$$

which is the basic expression from which most resistance calculation methods are derived.

2.1.2   Thermal Resistance of Gases and Fluids

When making a thermal model representation of air, convection is a heat transfer process that needs to be considered. The modelling of air is a complex matter since fluid motion is dependent on so many factors, such as rotational speeds, surface structure, geometry dimensions, forced flow, etc. The thermal resistance between a solid surface and the ambient fluid can be written on the form

$$R = \frac{1}{\alpha A} \tag{6}$$

where A is the surface area subjected to convection, and α is the so called *heat transfer coefficient* $[W/m^2C]$.

Finding α can be a challenging task requiring detailed knowledge of the machine. Achieving good values on some coefficients requires *Computational Fluid Dynamics* (CFD), a FEM based method demanding a lot of effort and expertise. Such detailed knowledge is however not always necessary for our "everyday" design requirements [5]. Instead, it is often calculated by using formulas based on empirical studies. The behaviour of the movement of the air can be described by a few dimensionless numbers. The Nusselt number (Nu), the ratio of convective to conductive heat transfer normal to the boundary, is perhaps the one most closely related to the heat transfer coefficient. The relation with α can be written as

$$\alpha = \frac{\lambda_{Air} \mathrm{Nu}}{2L} \tag{7}$$

Nu $= 2$ corresponds to a laminar flow, meaning that the molecules are only moving perpendicular to the normal of the plane. When that is the case, (6) becomes the same as for any solid, which is seen if inserting (7) in (6).

Nusselts number tend to be high for high rotor speeds and uneven surfaces, since those parameters increase turbulence. Several papers have made thorough investigations on how these parameters relate to each other for electric motors of different sorts, shapes and sizes for different points of operation. The chosen model is presented in Section 3.3.2.

2.2   Solving Heat Transfer Problems

Two ways of solving the heat transfer problems are presented in this thesis. There is the *Thermal Resistance Network Modelling*, which is a quick method based on the fundamental heat transfer mechanisms for simplified machine elements. There is also the much more computationally intense *Finite Element Method*, which is potentially very accurate provided good input data.

2.2.1   Thermal Resistance Network Modelling

To find out the steady state behaviour of a thermal system, it can be represented with a network consisting of thermal resistances, heat flow and temperature sources. The conductance matrix of a system consisting of $n + 1$ nodes will look like

$$\boldsymbol{G} = \begin{bmatrix} \sum_{i=1}^{n} \frac{1}{R_{1,i}} & \frac{-1}{R_{1,2}} & \cdots & \frac{-1}{R_{1,n}} \\ \frac{-1}{R_{2,1}} & \sum_{i=1}^{n} \frac{1}{R_{2,i}} & \cdots & \frac{-1}{R_{2,n}} \\ \vdots & \vdots & \ddots & \vdots \\ \frac{-1}{R_{n,1}} & \frac{-1}{R_{n,2}} & \cdots & \sum_{i=1}^{n} \frac{1}{R_{n,i}} \end{bmatrix} \tag{8}$$

Let a loss vector be defined to represent the power loss injected in each node,

$$\boldsymbol{P} = \begin{bmatrix} P_1 \\ P_2 \\ \vdots \\ P_n \end{bmatrix} \tag{9}$$

and corresponding temperature vector

$$\boldsymbol{\Theta} = \begin{bmatrix} \theta_1 \\ \theta_2 \\ \vdots \\ \theta_n \end{bmatrix} \tag{10}$$

representing the increase in temperature compared to the ambient temperature. $\boldsymbol{\Theta}$ can be calculated by inverting the conductance matrix and multiplying it with the power vector, and thus getting an expression derived from ohm's law,

$$\boldsymbol{\Theta} = \boldsymbol{G}^{-1}\boldsymbol{P} \tag{11}$$

Although setting up an accurate thermal network may require some work, the resulting model provides a means of getting quick solutions to changes in input parameters, since the mathematical complexity and number of necessary computations are low. The time taken to set up the model depends on the level of detail and accuracy needed for the engineering problem at hand [2, p.2]. The process of finding the equivalent thermal resistances for some general geometrical shapes is described in Section 2.3.3.

2.2.2   FEM Analysis

FEM stands for *Finite Element Method*, and is a very important tool when it comes do dynamic systems such as structural mechanics and thermodynamics[6]. Most systems and processes around us can be described as being of a continuos nature. Mathematically such a system can be represented by differential equations, which can sometimes be rather complex to solve. It is therefore desirable to have a method of making the problem less complex, while still being able to get notion of local effects and variations.

The basic principle is that such a system is divided into a number of more easily manageable and well defined elements. If the number of elements were allowed to increase and approach infinity, that would correspond to a continuous system which would theoretically be very accurate, though unfortunately also tedious to solve. By approximating it with a limited number of elements however, one can achieve a mathematical problem of arbitrary accuracy and requiring a more moderate amount of computations. The different elements are all assigned a set of equations and starting state. A numerical solution can then be acquired when all of these element equations have been assembled into a single system, and solved for when each node is in equilibrium.

In the case of the FEM simulations in this report, they will essentially solve the equation of conduction presented in 2.1.1. Air will be modelled just as any solid, while the convection is considered by scaling the thermal conductivity according to the same equations as the for network model described in section 3.3.2.

2.3   Thermal Network Modelling Methods

When a thermal resistance network is set up, there are many questions regarding for instance how to simplify the object in question, where to place the nodes, and how equivalent thermal resistances can be calculated for different shapes. This section presents principles and equations for developing a thermal network.

2.3.1   Nodalization

If a real object is to be represented with a circuit model consisting of a finite number of elements, some simplifications must inevitably be made. Nodalization is the concept of dividing an object into subelements, where each element or connection point is represented by no more than one or possibly a few nodes. The notion of *lumped parameter modelling* means the simplified representation of the properties of the body in more manageable entities, such as average temperature, volume, and thermal mass.

An object may principally be divided into nodes in an arbitrary way, though there are naturally many things that should be taken into consideration. Some of these factors are where you need an accurate temperature prediction, what the expected temperature distribution looks like, and the ease of calculations of the resulting geometry. It can also be that a node needs to be placed somewhere where the point in itself is not of interest, but a connection is needed between other nodes or to increase the accuracy in the modelled flow path. Sticking to basic geometrical shapes makes the calculations of areas and volumes easy to calculate. In the case of the model being compared with actual measurements, it is advantageous to place nodes close to where the physical sensors are positioned[2, p.5].

The number of nodes can be chosen by the model designer based on the requirements on the resolution of the model. More nodes means getting more detailed information on different parts of a single section, or of a higher number of parts of an object. The price of having the extra accuracy of more nodes is an addition to the complexity of the network to analyse. Provided that the body is somewhat homogenous, making an interpolation between the temperatures of two adjacent nodal points can be a way of achieving acceptable estimation [2, p.4].

2.3.2   Node Location in Geometry

Heat that flows homogeneously from the inner to the outer boundary of a hollow cylinder can analytically and exactly be calculated using the thermal version of Ohms law. Modelling an object where the heat generation is distributed over the whole body is a more complicated matter. Two criteria govern the choice of node location in this situation:

1. Accurate prediction of ΔT over the body.

2. Accurate prediction of the temperature at a point of interest, for instance a potential hot spot.

In some simple objects, such as a bar which can be considered thermally isolated on all but both ends, achieving both criteria is possible. For a body where thermal resistance and volume per unit length do not vary in the same way along the heat path, it becomes more complicated. One such case is the

radial path through a cylindrical object, which is an often recurring basic shape when modelling an electric motor. Figure 2 shows the relationship of the "accumulated" volume (which is proportional to the loss if uniformly distributed) and the "remaining" thermal resistance for a hollow cylinder.
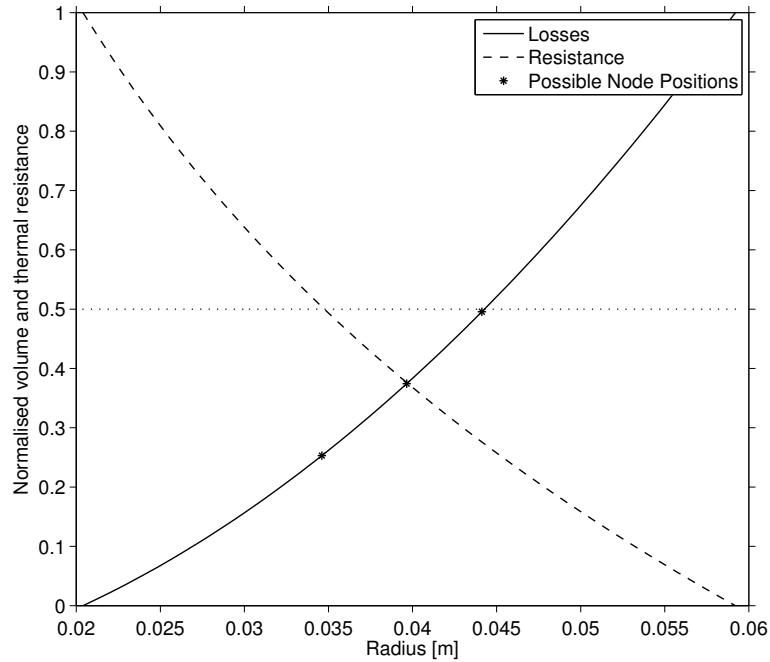
Figure 2: The accumulated losses and remaining thermal resistance for radial heat flow in an object similar to the rotor, as a functions of the radius.

By dividing the object into an infinite amount of smaller bodies, one can know the exact heat accumulated at each radii, and the exact resistance that heat has left to pass through. Although obviously never as high as infinity, the high discretisation level of the FEM solution allows it to be accurate in such cases. When it comes to the thermal resistance modelling, simplicity is important and it is desirable to end up using a network with a low number of nodes. The question is then; at which radii is it most suitable to inject the losses, if only one node is placed in the body, and how large is the approximation error?

Lets start by defining three radii of interest. The *resistive midpoint*, is the point along the heat path through a body where half of the total resistance is passed, and half is left to go. In the case of a hollow cylinder, the equivalent radius is named r_{resMid} and corresponding node n_{resMid}. The *geometrical midpoint* is simply the mean of the inner and outer radii, and is labelled as r_{radMid} and n_{radMid}. Finally, the *volumetric midpoint* is where the half of the objects total volume is passed, and likewise also the point where half

of losses are generated at either side. The corresponding parameters are r_{volMid} and n_{volMid}.

To find out r_{resMid}, (15) is used to derive an expression for the specific radius where the inner and the outer segment have the same thermal resistance. The resulting expression is

$$r_{resMid} = \sqrt{r_i r_o} \tag{12}$$

where r_i is the inner radius and r_o is the outer radius. As for r_{volMid}, it can be determined to

$$r_{volMid} = \sqrt{\frac{r_i^2 + r_o^2}{2}} \tag{13}$$

The principle of placing the node at r_{resMid} or r_{volMid} is further illustrated in Figure 3. The convention in these situations seem to be placing the node in the resistive midpoint, which is most probably due to the fact that it is most easy to calculate it that way. But which is the most suitable option in general is not obvious and will be investigated closer for a few relevant cases in the case study in Section 2.4.2.
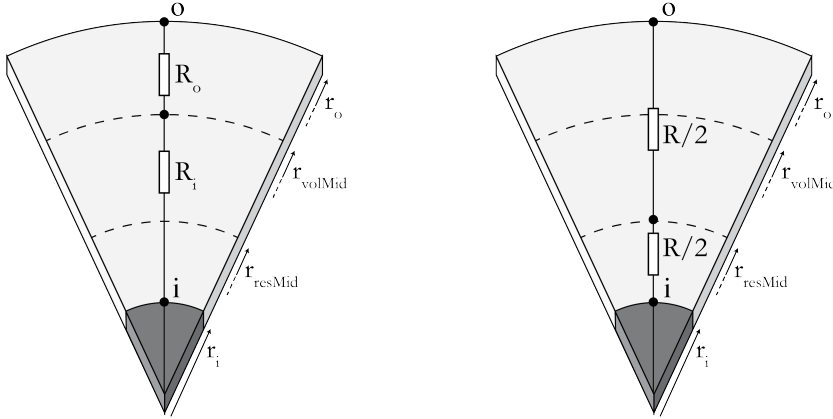
(a) Placing the node on the volumetric midpoint.

(b) Placing the node on the resistive midpoint.

Figure 3: Figure showing the difference between placing a node at r_{resMid} and r_{volMid} in a slice of an object similar to a section of a rotor.

2.3.3   Resistance Calculation Methods for General Geometries
Through simplifications and division into basic elements, a complex geometry can usually be described using expressions for the thermal resistance of a few general shapes. Here follows the derivation of a few thermal resistance calculation methods for some basic shapes than can be found in a motor.

Hexahedrons

A hexahedron is a variation of a cuboid with 6 faces, where all angles are not necessarily orthogonal. An example could be the geometrical body you would get if you would start with a cuboid as described in (4), but during the path along the length alter the width or the height. The thermal resistance of such an object could be described by

$$R = y \frac{ln\left(\frac{x_o}{x_i}\right)}{l\lambda(x_o - x_i)} \tag{14}$$

where l is the thickness, λ is the thermal conductivity, x_i is the inner width, x_o is the outer width, and y is the length of the path of integration. An example of this figure is seen in Figure 4
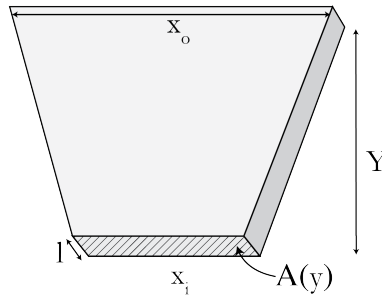
Figure 4: Example of a hexahedron with a variable width x.

Hollow Cylinders

Applying (5) for a disk shaped object in a cylindrical coordinate system yields

$$R = \frac{ln\left(\frac{r_o}{r_i}\right)}{2\pi l\lambda} \tag{15}$$

where the radius varies between r_i and r_o. For a segment of such a cylinder, like the one depicted in Figure 5 the resistance is scaled by the angle ϕ of the segment as presented in

$$R = \frac{2\pi}{\phi} \frac{\ln\left(\frac{r_o}{r_i}\right)}{2\pi l\lambda} \tag{16}$$
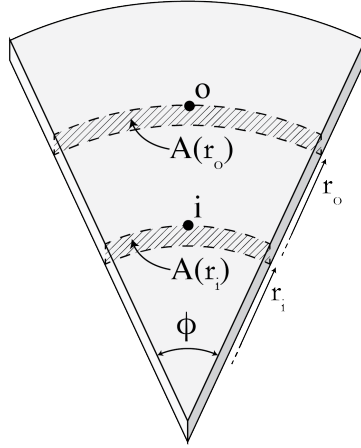
Figure 5: Nomenclature of a segment of a thin cylinder, where integration takes place from r_i to r_o.

For heat flow in the same kind of hollow cylinder or hollow cylinder segment but for the circumferential direction rather then the radial, the thermal resistance is different. Let the heat flow path be defined as a line along the mean radius. The base of integration in (5) is changed to the angle θ, which is swept along the full angle ϕ of the cylinder segment. The base change then becomes

$$\mathrm{d}l_{path} = \mathrm{d}\theta \frac{r_o + r_i}{2} \tag{17}$$

For constant cross sectional area $A(\theta) = (r_o - r_i)l$, the resulting expression for the thermal resistance is

$$R = \frac{\phi}{2\lambda l} \frac{r_i + r_o}{r_o - r_i} \tag{18}$$

The integration and variables are visualised in Figure 6.

Hollow Cylinder Segments With Varying Angle
The shape in Figure 7 can be interpreted as a circular segment where the angle change along the radius. Letting the angle in the integration leading to (16) change linearly according to

$$\theta(r) = \theta_i - \frac{\theta_i - \theta_o}{r_o - r_i}(r - r_i) = ar + b \tag{19}$$
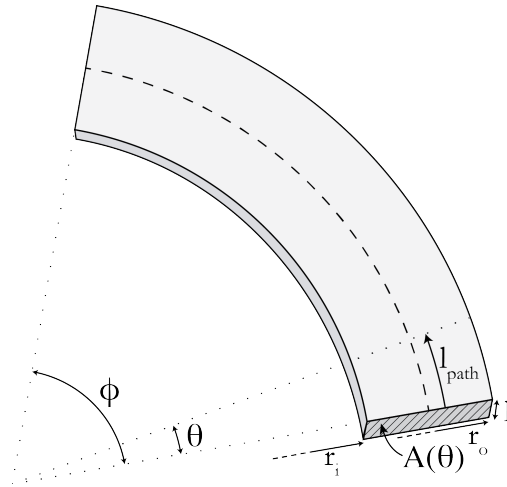
Figure 6: Calculation of circumferential heat flow in a thin, hollow cylinder by assuming constant r but changing angle.

results in

$$R = \frac{1}{\lambda l b} \ln \left(\frac{r_o}{r_i} \frac{a r_i + b}{a r_o + b} \right)$$

(20)

where a and b are as defined in (19).
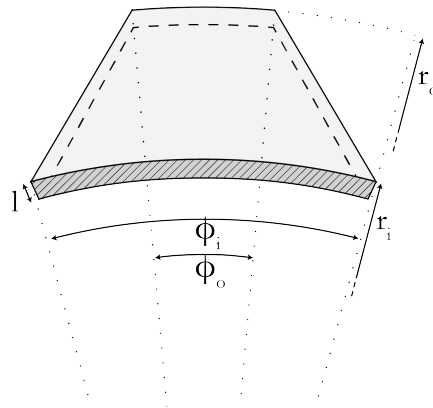
Figure 7: Nomenclature of a thin cylindrical segment, where angles vary along the radius.

2.4   Case Studies

Which choice of simplification or method to use is not always apparent. Here follows two case studies, where it is investigated which resistance calculation method and which node placement strategy yields the best results for dimensions similar to those in the actual machine geometry, but with other factors that could obstruct the analysis removed.

2.4.1   Choice of Resistance Calculation Methods

All equations described above assumed that the heat flow is only taking place in one direction. Though not necessarily entirely true in reality, it is required in order to keep the complexity down. To get an idea of how large the error from this simplification might be, and also see how significant the estimation error from further approximations might be, a few cases will be simulated in ANSYS and compared with analytical calculations. The FEM solution is well suited for this kind of calculations and can be assumed to be quite accurate.

Each test is set up by modelling a certain object of a similar shape and dimensions to what might be found in the motor. A constant temperature is set at the inner and outer surfaces as boundary conditions, and then it is seen what the resulting heat flow through the object is. The corresponding resistance can be calculated according to (1), and is compared to the analytically calculated values. The initial parameters before sweeping are listed in Table 2. When approximating the shapes as cuboids, the equivalent integration length is $r_o - r_i$, and width is determined to $x = \phi r_{avg}$, where r_{avg} is the mean radius.

Table 2: Parameters used in the simulation of the hollow cylinder segments.

Parameter	Value
l	1 mm
λ	1 W/mK
T_i	60 °C
T_o	22 °C
r_i	60 mm
r_o	90 mm
ϕ	0.6 rad

Approximating Cylinder Segment as Cuboid

This study is about seeing how well (16) and (4) approximate the thermal resistance of a section of a hollow cylinder, such as the one in Figure 6. That is to say, if a cylinder is simplified as cuboid for the sake of making

the thermal resistance calculations easier, how much is then the accuracy affected?

In Figure 8, the relative error between the FEM-results and the two analytical calculation results are shown when the angle of the cylinder segment is varied. It can be surmised that the magnitude of the error is not affected, hence it does not influence the choice of calculation method.

In Figure 9, it is instead the outer radius that is varied. It is clear that (16) gives a very accurate value on the thermal resistance, whereas the error in (4) becomes noticeable when the difference between r_i and r_o increases. For cylinder segments where $r_i \approx r_o$ the difference appear to be minimal. The situation with a 3.3% larger outer radius resulted in less than 0.1% increase in the perceived resistance.
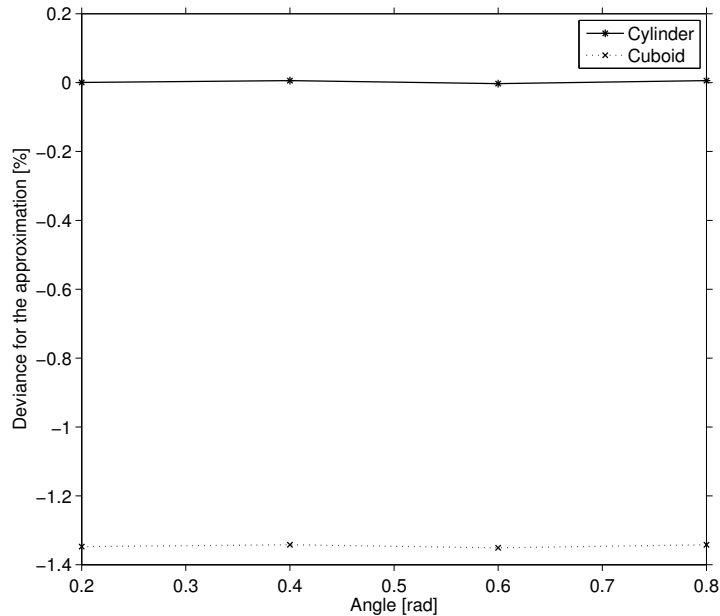
Figure 8: Investigating the influence of the angle of the object.

Approximation Methods for Circle Segments of Varying Angle
Now lets compare (20) and (14) instead, the equations for varying angles and widths. The parameters in Table 2 are used, with the exception for $\phi_i = 0.4$ while the outer angle is swept.

Figure 10 shows the results, which turn out to be in much less agreement and more difficult to draw strong conclusions from. In those situations where the angle narrows down further out, it appears to be best to simplify the shape using straight lines and use (14). When it instead widens to roughly 1.5 times the initial angle or more, (20) results in a better approximation.
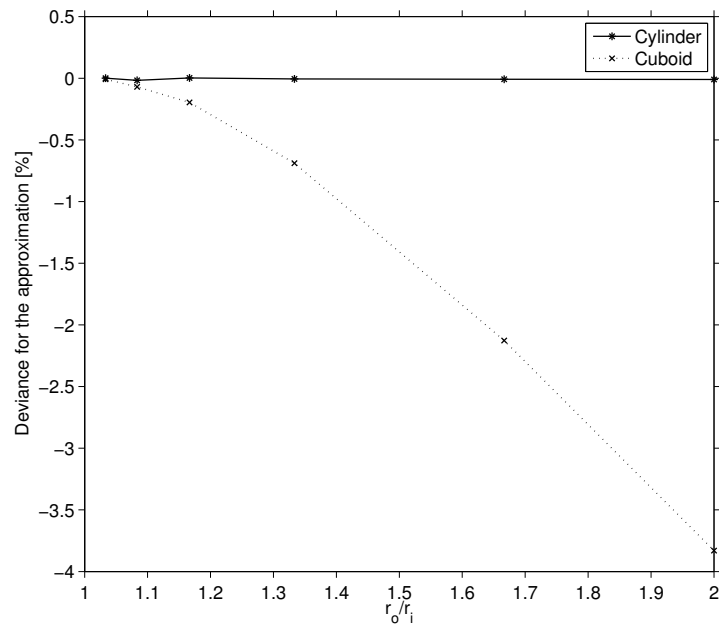
Figure 9: Investigating the influence of the length of the object by changing the outer radius
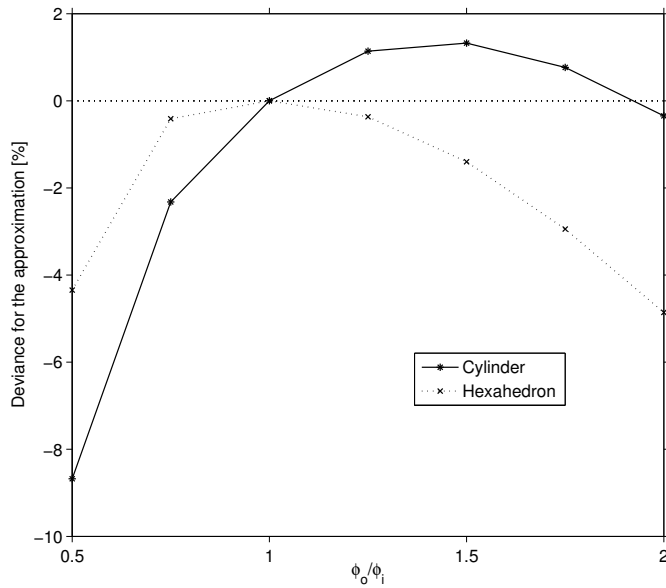
Figure 10: The deviance from the actual value when approximating the thermal resistance of a cylinder segment where the angle is changing along the radius.

Choosing Calculation Methods for the Stator Teeth

As have been seen in the previous case studies, the choice of calculation methods can have some importance even for simple geometries. The stator teeth have a more complex shape, although the most prevalent way of modelling it appear to be to be using mostly straight angles. It will here be investigated whether this model would be significantly improved by modelling it as sums of cylinder segments rather than cuboids and hexahedron. Figure 11a illustrates the simplified tooth geometry, while 11b shows a suggested segmentation of tooth using cylindrical segments.
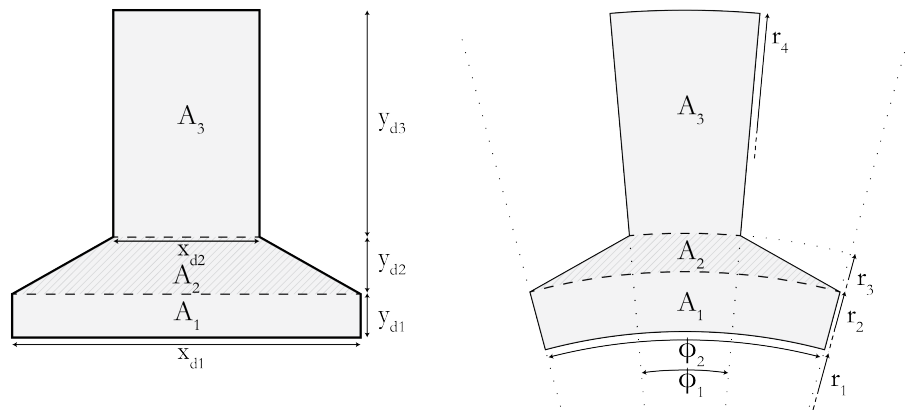
(a) Stator tooth geometry approximated using straight lines.

(b) Stator tooth geometry approximated using cylindrical segments.

Figure 11: Comparison of a stator tooth geometry for thermal resistance calculation using two methods

The simulation is set up in the same way as the previous cases, according to the parameters shown in Table 3.

Table 4 shows a comparison of the results when calculating the thermal resistances for each segment of the tooth and then adding them up. The equivalent resistance from the FEM-simulation turned out differently if simulated segment wise than for the whole tooth simulated at once, and both results are presented.

It turns out that for segment 1 and 3, it matters little which method is used. The major difficulty is segment 2, for which the error is roughly 15% in all cases. Adding all segments together, the uncertainty of the total tooth resistance is between 4.7-9.1 % for the best and the worst cases respectively if considering both the choice of calculation method and the uncertainty in the FEM-solutions. The difference between the choices of methods however was at most 1.3 %.

Table 3: Parameters used in the simulation of the tooth

Parameter	Value
l	1 mm
λ	$1\ W/mK$
T_i	$60\ °C$
T_o	$22\ °C$
r_{t1}	60 mm
r_{t2}	63 mm
r_{t3}	69.5 mm
r_{t4}	81.8 mm
ϕ_{t1}	0.64 rad
ϕ_{t2}	0.64 rad
ϕ_{t3}	0.3329 rad
ϕ_{t4}	0.2942 rad

Table 4: Comparison of the results from approximating the tooth using cylindrical shapes and square shapes

Method	Equation	Resistances [K/W]			
		A1	A2	A3	Total
Cylinder segment	(16)	76.2	201.9	519.7	797.8
Cylinder segment, $\phi = f(r)$	(20)	76.2	207.9	519.5	803.6
Cuboid	(4)	76.2	201.7	518.5	796.4
Hexahedron	(14)	76.2	210.1	521.2	807.5
FEM		76.2	248.1	522.7	847.0
FEM – As one object					876.2

Conclusions

It can be said that all investigated analytical equations approximate the resistance of a hollow cylinder segments where $r_i \approx r_o$ with very high accuracy. For shapes where the width varies, some approximation error seem unavoidable. The difference however is small enough for it not to matter much in most cases. When looking at the 2nd and 3rd segments of the teeth, the best results was achieved using (14), so that is what will be used for those objects in the thermal network calculations.

2.4.2   Node Location in Hollow Cylinders

To investigate how much the choice of where to inject the losses may actually affect the calculated temperature drop over the object, a very simple simulation of hollow steel cylinders with internal heat generation is set up. Nodes are placed at r_i, r_{resMid}, r_{radMid} and r_{volMid}. It is then tested to see

what the temperature would be when choosing only one of them at a time to inject all the losses.

Two cylinders are tested to see the influence of the r_o/r_i ratio. One is of similar size and shape as the machine rotor, and the other corresponds to the stator. By simplifying the setup to this extent rather than applying the changes to an ordinary machine simulation, it is easy to investigate the node location without getting confused from the influence of other uncertainty factors such as circumferential flows. The parameters for these cylinders are presented in Table 5. The loss data and thickness is chosen for convenient calculations, and the temperatures in the following simulations are not comparable with whose from the actual machine simulation.

Table 5: Parameters used in the node placement case study.

Parameter	Rotor like cylinder	Stator like cylinder
l	1 mm	1 mm
λ	1 W/mK	1 W/mK
Injected loss	1 W	1 W
T_o	22 $°C$	22 $°C$
r_i	20.3 mm	60 mm
r_o	59.3 mm	95 mm

The results from the simulations can be seen from the plots in Figure 12, and for more detailed data please see Appendix B.1. The difference between the node placement options is significant. The choice that appear to lead to the largest approximation error of the ones tested is placing all the losses in the n_{resMid}, for which the predicted temperature increase is 48.7 % and 17.5 % for the two cases. The node placement yielding the most correct temperature prediction is the at r_{radMid}, for which the given temperature is 10.8 respectively 4.1 % higher than according to the FEM simulation.

Conclusions

This case study presumes a 1-dimensional heat flow, and investigates a case where all heat being generated internally rather than coming from an inner node. If a considerable heat flow is coming from an inner node, the impact would not appear to be as significant as is implied by Figure 12, and if heat has more than one outlet the (which might be the case when axial flows is considered), the best choice could possible be a different one. That being said, the following conclusions can be drawn.

- For a hollow cylinder such as the ones described in this case study, the node position that will yield the most accurate temperature prediction is r_{radMid}, or somewhere between r_{radMid} and r_{volMid}.
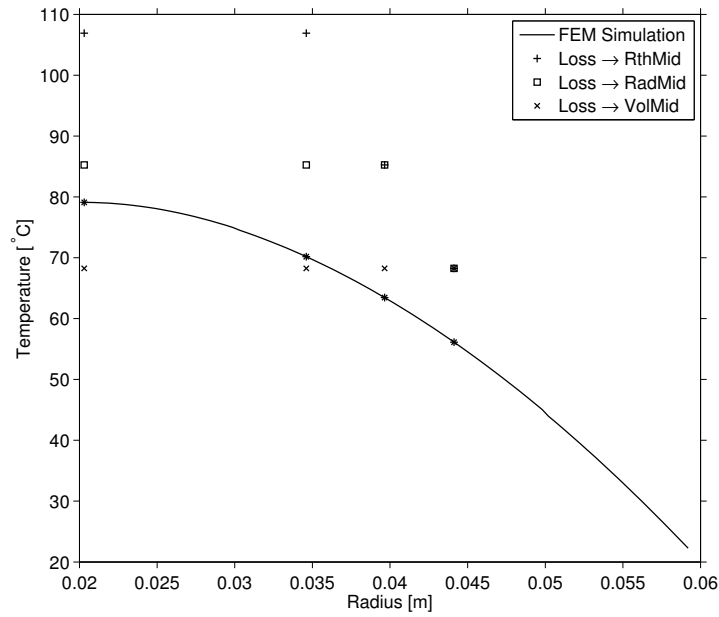
(a) Object similar in shape to the rotor.
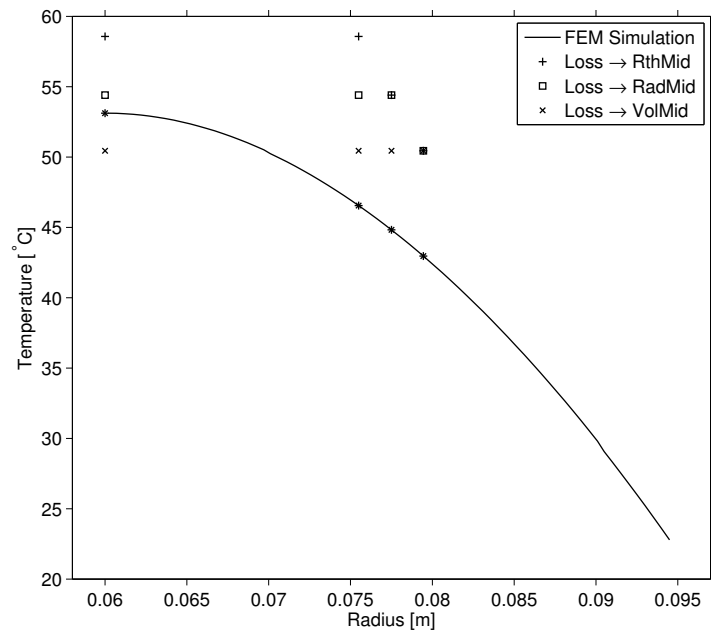
(b) Object similar in shape to the stator.

Figure 12: The simulated temperature distribution at different radii for different choice of loss injection nodes for an object similar to a rotor, compared with a FEM solution. Most important is the temperature at the inner radius.

- The r_o/r_i ratio has large impact on the volume/resistance curves shown in 2, and therefore the error from injecting the losses in a non-optimal point.

- The temperature given at the node where the losses are injected will overestimate the temperature contribution from the body itself. Assuming that the temperature at the radius of the node is well represented by the node temperature is only valid if the internally generated heat is low compared to the heat flow from inner nodes.

3   The Thermal Model

In this chapter the design of the machine is presented along with the proposed models and inputs. Based on the intended node locations, the machine can be divided into subelements for which the the thermal resistances are calculated the assumptions regarding the modelling explained. The thermal resistances are in other words to begin with treated in respect to their geometrical bodies in question, and will be referred to in Section 3.4 where the equivalent node-node resistances are presented for both a high resolution and a low resolution network. That means that in some cases several ways of calculating a geometrical resistance will be presented.

3.1   The Machine Design

The model is based on a water cooled PMSM with double layered concentrated windings and interior magnets. The machine dimensions can be looked up in Table 6. Clarifications on what some of the variables symbolise is shown in Figure 13.

The materials used in each respective machine part is shown in Table 7, while the material properties can be found in Table 8. For those whose thermal conductivity will be simulated as temperature dependent, the values will be given at several temperatures and the values in between are interpolated.

The thermal conductivity of the stator and rotor iron material, NO20, should be commented. In some published papers [1, 7], the value given is that for the actual iron, while the lamination materials heat conductivity is neglected. The implications that follow for the conductivity of the material mix is accounted for by scaling down the equivalent axial length by the lamination filling factor. The value given in Table 8 is taken from the product data sheet and takes into account the restrictions posed by the lamination material, and so does not need further scaling.

Table 6: Machine dimensions

Symbol	Value	Description
n_m	6	Number of magnets
n_s	9	Number of stator slots
l_a	200 mm	Axial length
r_{sh}	20.3 mm	Shaft radius
w_m	33 mm	Magnet width
h_m	5 mm	Magnet thickness
r_{mi}	49.2 mm	Inner magnet radius
r_{mo}	54.2 mm	Outer magnet radius
ϕ_m	37.1°	Magnet angle
ϕ_{mAir}	46°	Magnet air angle
ϕ_{rSym}	60°	Rotor symmetry section angle
r_{ro}	59.3 mm	Outer rotor radius
h_{FeMin}	1 mm	Minimum iron thickness around magnets
h_g	0.7 mm	Air gap, @T_{amb}
r_{sti}	60 mm	Inner stator radius
r_{t1}	60 mm	1st tooth segment inner radius
r_{t2}	63 mm	2nd tooth segment inner radius
r_{t3}	69.5 mm	3rd tooth segment inner radius
r_{t4}	81.8 mm	4th tooth segment inner radius
ϕ_{s1}	3.3°	Slot angle @ r_{t1}
ϕ_{s2}	3.3°	Slot angle @ r_{t2}
ϕ_{s3}	20.9°	Slot angle @ r_{t3}
ϕ_{s4}	23.1°	Slot angle @ r_{t4}
ϕ_{t1}	36.7°	Tooth angle @ r_{t1}
ϕ_{t2}	36.7°	Tooth angle @ r_{t2}
ϕ_{t3}	19.1°	Tooth angle @ r_{t3}
ϕ_{t4}	16.9°	Tooth angle @ r_{t4}
d_i	0.4 mm	Slot insulation thickness
γ_{sFill}	0.45	Slot fill factor
h_y	13.1 mm	Yoke thickness
r_{sto}	95 mm	Outer stator radius
h_f	7 mm	Equivalent frame thickness
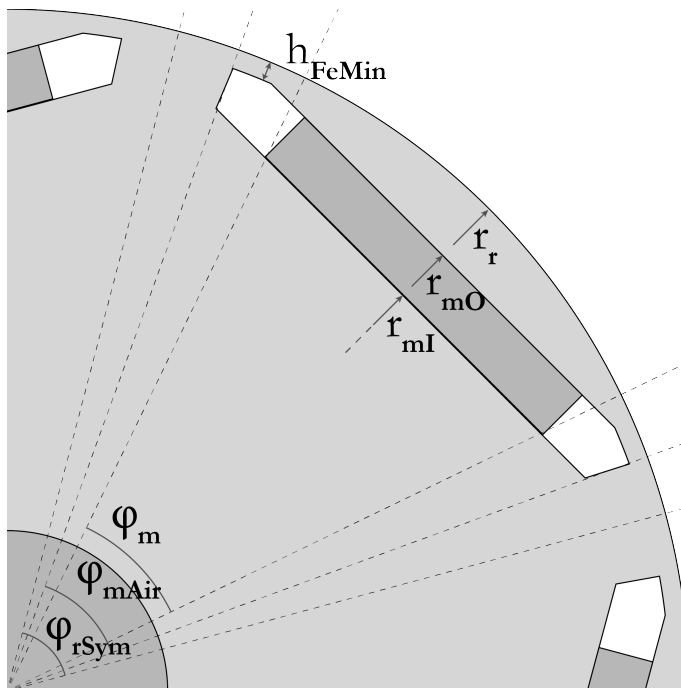
(a) Nomenclature for the rotor.
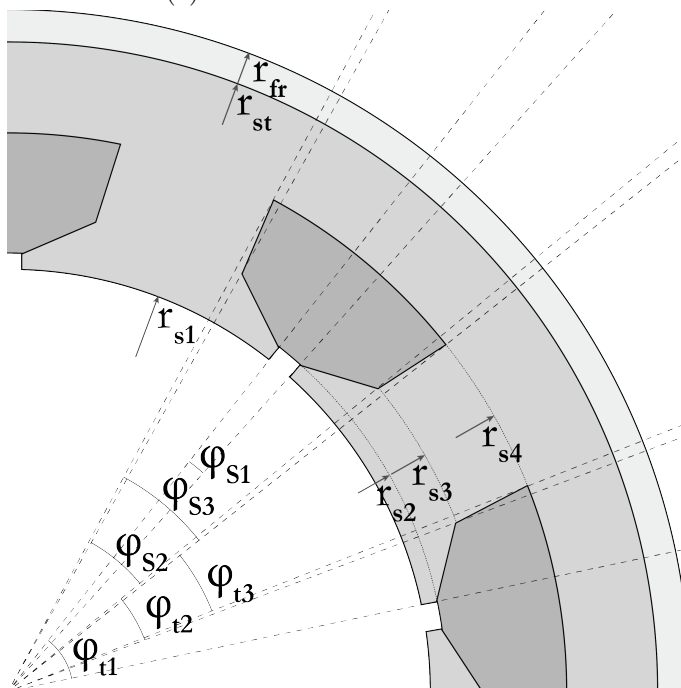
(b) Nomenclature for the stator.

Figure 13: The nomenclature for some important angles and radii.

Table 7: The materials of different parts of the machine

Machine Part	Materials
Rotor core	NO20
Stator core	NO20
Shaft	Steel
Windings	Copper
Frame	Aluminium
Magnets	NdFeB
Slot insulation	Mylar film
Winding impregnation	Unsaturated polyester

Table 8: The thermal conductivity of the materials in the machine.

Material	Thermal Conductivity [W/mK]		
	$25°C$	$125°C$	$225°C$
NO20 – radial direction	28		
NO20 – axial direction	0.37		
Copper	401	400	398
Aluminium	205	215	250
NdFeB	9		
Air	0.0257	0.0328	0.0404
Mylar film	0.2		
Unsaturated polyester	0.2		

3.2 Proposed Node configurations

Two thermal networks models are proposed. They are essentially based on the same principles but consist of a different number of nodes. The idea is that increasing the resolution of the network will not only give a more detailed description of the temperature distribution in the motor, but ideally also be able to more accurately model the different heat flow paths in the motor and the associated resistances.

The first model consists of few nodes and will be referred to as the *simple network*.The node placement is mostly consistent with that in [1, 5, 7] et al., with the exclusion of non-radial phenomena. The main difference lies in the way some of the connecting resistances are calculated. Figure 14 shows how the nodes have been placed in the motor. The position of nodes marked with a square are determined in $[r, \phi]$, whereas a circle marks nodes only defined by $[r]$. The air gap for instance is marked with a circle as it is assumed to have a uniform temperature at that specific radius. The tooth node on the other hand represents the temperature at the middle of the tooth at a specific radius, and is thus marked with a square. In the figure some aspects have been exaggerated for visual clarity.

The second node configuration is denoted as the *complex network* due to the higher number of nodes. It differs from the first in that several nodes have in some cases been placed in machine parts with considerable heat flows in several directions, large temperature gradient, which makes them more difficult to model accurately. The node configuration can be seen in Figure 15.

Some of the thermal resistances are the same for both networks. When they are not, the ones associated with the simple network have the subscript S, and the one referring to the complex network C.
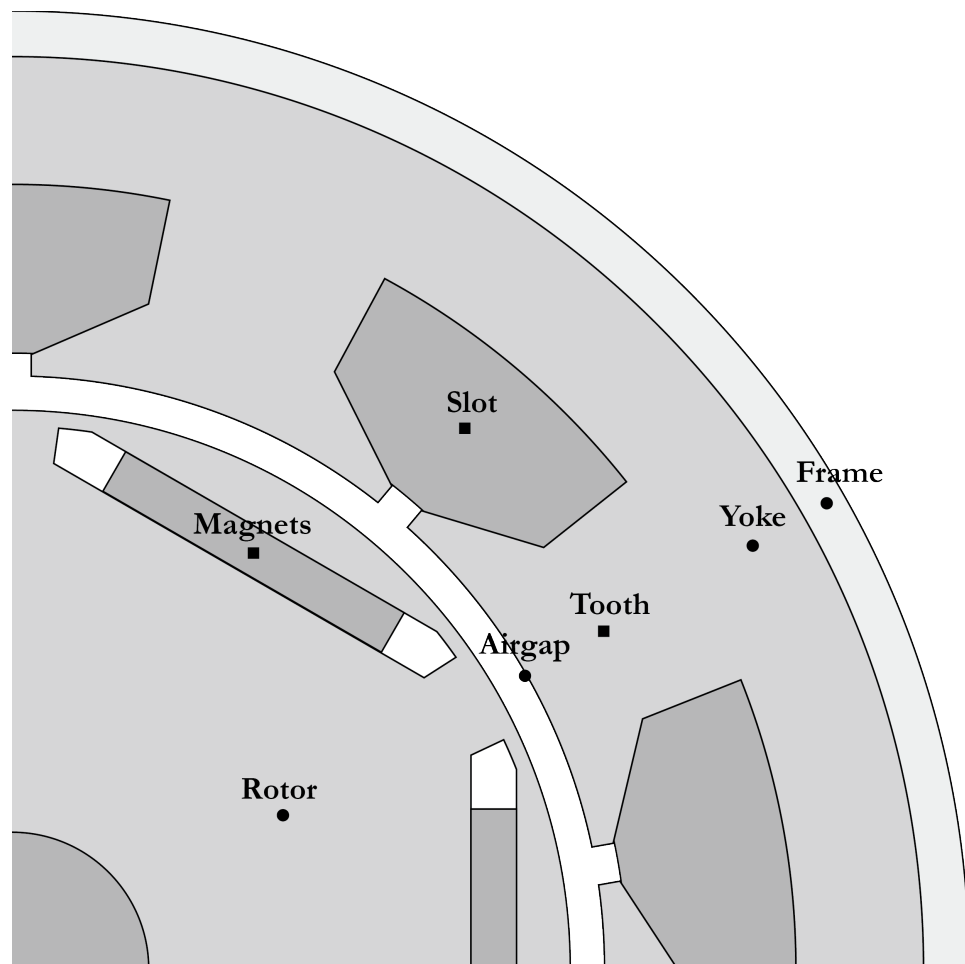
Figure 14: The node placement for the simple thermal network.
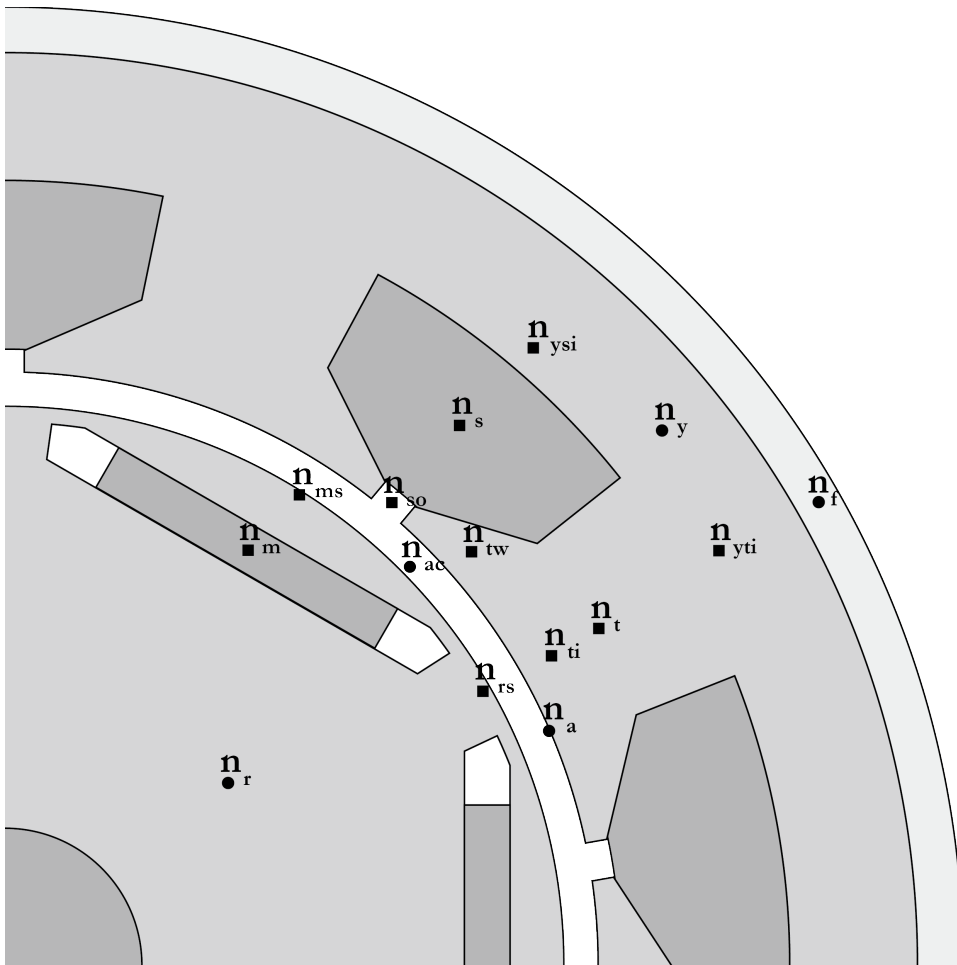
Figure 15: The node placement for the complex thermal network.

3.3 Thermal Resistances for Machine Parts

The following is an account of how each part of the machine is treated when it comes to thermal resistance calculations. For the cases where the two node configurations differ, two ways of dividing the part in subelements are presented.

3.3.1 Rotor

Two rotor segmentations are suggested. Both make convenient approximations to the shape and dimensions of the rotor, but to different extents. The first and most simple division is an adaptation of the rotor model presented in [8]. It is assumed that there is no circumferential heat flow, and consequently temperature varies only in the radial direction. The other takes into account that heat flow take two different paths from the rotor centre out to the air gap; through the magnets or around them, and that will result in a circumferential temperature gradient. Illustrations pointing out the differences are shown in Figure 16.

All segments are numbered and have their associated resistances explained in Table 9 and 10 respectively. Note that some are just for one fraction of the machine, while other are for a full turn around rotor.

The thermal resistance of the air surrounding the magnets is approximated as infinite, since simulations have established that the impact on the temperature by including them was less than $1/100°C$.
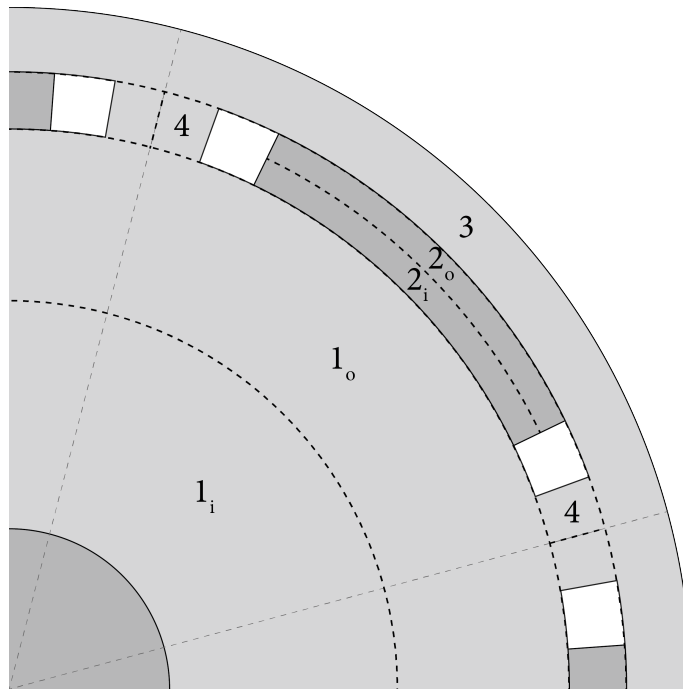
(a) Dividing the rotor into segments for the low complexity network.
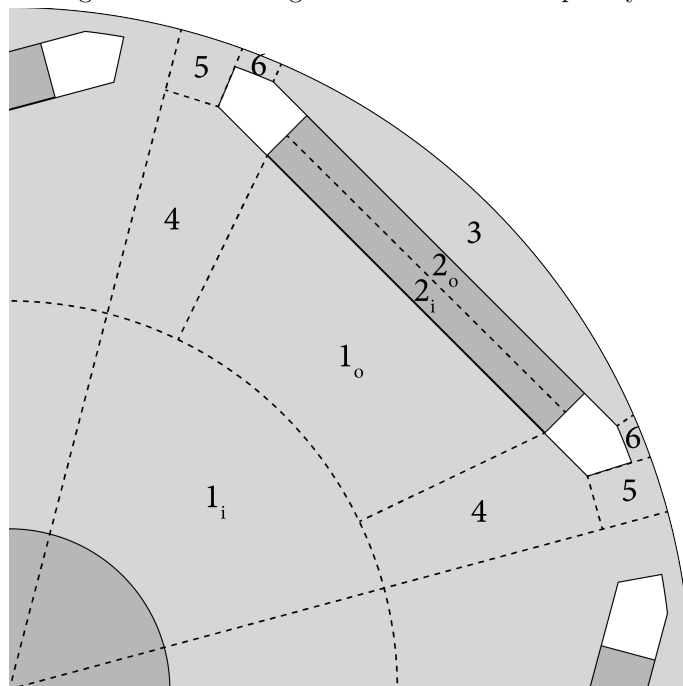
(b) Dividing the rotor into segments for the high complexity network.

Figure 16: Two ways of dividing the rotor into manageable segments for thermal resistance calculation.

Table 9: Equations behind the thermal resistances in the simple rotor model shown in Figure 16a.

		Input		
Resistance	Equation	Inner radius	Outer radius	Angle
R_{rS1i}	(15)	r_{sh}	r_{node}	2π
R_{rS1o}	(15)	r_{node}	r_{mi}	2π
R_{rS2i}	(16)	r_{mi}	$\frac{r_{mi}+r_{mo}}{2}$	ϕ_m
R_{rS2o}	(16)	$\frac{r_{mi}+r_{mo}}{2}$	r_{mo}	ϕ_m
R_{rS3}	(15)	r_{mo}	r_r	2π
R_{rS4}	(16)	r_{mi}	r_{mo}	$\frac{\phi_{rSym}-\phi_{mAir}}{2}$

Table 10: Equations behind the thermal resistances in the complex rotor model shown in Figure 16b.

		Input		
Resistance	Equation	Inner radius	Outer radius	Angle or Width
Radial direction				
R_{rC1i}	(15)	r_{sh}	r_{node}	2π
R_{rC1o}	(15)	r_{node}	r_{mi}	ϕ_m
R_{rC2i}	(4)	r_{mi}	$\frac{r_{mi}+r_{mo}}{2}$	w_m
R_{rC2o}	(4)	$\frac{r_{mi}+r_{mo}}{2}$	r_{mo}	w_m
R_{rC3}	(16)	r_{mo}	r_r	ϕ_{mAir}
R_{rC4}	(15)	r_{node}	r_{mi}	$\frac{\phi_{rSym}-\phi_m}{2}$
R_{rC5}	(16)	r_{mi}	r_r	$\frac{\phi_{rSym}-\phi_{mAir}}{2}$
R_{rC6}	infinite			
Circumferential direction				
R_{rC3-cf}	(18)	r_{mo}	r_r	ϕ_{mAir}
R_{rC6-cf}	(18)	$r_r - h_{FeMin}$	r_r	$\frac{\phi_{mAir}-\phi_m}{2}$

3.3.2   Air Gap

Section 2.1.2 describes how to calculate the heat transfer through a gas given a set of dimensionless numbers. To determine these parameters, a model presented in [5, p.3546] will be used, which consist of a set of equations that can be used to calculate the Nusselt number at a given speed. To start with, Taylor's number (the ratio between centrifugal forces due to rotation and the viscous forces) is written as

$$\text{Ta} = \frac{\rho_{air}^2 \omega^2 r_g h_g^3}{\mu^2} \tag{21}$$

where ρ_{air} is the air density, ω is the angular speed, r_g is the radius in the middle of the air gap, h_g the air gap length, and μ is the dynamic viscosity

of air. A modified Taylor's number Ta_m is then defined as

$$\text{Ta}_\text{m} = \text{Ta} \frac{1697 \left[0.0056 + 0.0571 \left(\frac{2r_g - 2.304h_g}{2r_g - h_g} \right)^2 \right] \left[1 - \frac{h_g}{2r_g} \right]}{\pi^4 \left[\frac{2r_g - 2.304h_g}{2r_g - h_g} \right]} \tag{22}$$

The Nusselt number can then be approximated by

$$
\begin{aligned}
\text{Nu} &= 2 & (\text{Ta}_m < 1700) \\
\text{Nu} &= 0.128\text{Ta}_m^{0.367} & (1700 < \text{Ta}_m < 10^4) \\
\text{Nu} &= 0.409\text{Ta}_m^{0.241} & (10^4 < \text{Ta}_m < 10^7)
\end{aligned}
\tag{23}
$$

Additionally, there is the thermal expansion of the rotor to consider. As the machine temperature increases, the air gap becomes smaller according to

$$h_g = h_{g0} - \kappa_{Fe} r_g \Delta T \tag{24}$$

where h_{g0} is the initial air gap length, and κ_{Fe} is $10.4 \cdot 10^{-6}$, the thermal expansion coefficient for iron [1, p. 28].

Knowing these parameters, the air gap resistance R_g can finally be calculated from (6).

3.3.3 Slot Openings

The openings of the slots are generally not specifically addressed in literature. For the investigated machine they are rather large, and the thermal conductivity of air is low. The conductance becomes rather negligible for the low turbulence of low speeds, if the same scaling of the heat transfer as for the air gap is adapted. It is however conceivable that due to its shape, the turbulence of the air in the slot opening could be significant enough to warrant being modelled as a separate body connecting the ordinary air gap with the slots, even in the cases where the air gap flow is close to laminar.

Hence, two ways of setting the slot openings resistance are suggested in Table 11.

Table 11: Thermal resistance models for the slot openings

| Resistance | Equation | Input | | |
		Inner radius	Outer radius	Angle
$R_{sOpeningS}$	infinite			
$R_{sOpeningS-cf}$	infinite			
$R_{sOpeningC}$	(16)	r_{t1}	r_{t2}	ϕ_{s1}
$R_{sOpeningC-cf}$	(18)	r_{t1}	r_{t2}	ϕ_{s1}

3.3.4   Stator Slots and Windings

Modelling the stator slots is challenging, due to several phenomena that are difficult to generalise for different machines. The major of these can be summarised as:

- Slot insulation – Between the stator iron and the copper windings, there is a layer of insulation. The insulation itself adds a considerable contribution to the thermal resistance between stator and teeth. Additionally there are minor air pockets between the lamination and the stator sheets.

- Material mix – The copper windings are coated with impregnation, and in between each strand there is some other medium (air/grease/varnish). While the thermal conductance of the slots in the axial direction is basically the same as that of the copper windings, it is in the orthogonal plane dominated by numerous by the materials with lower conductivity.

- Internal Heat Generation (IHG) – The heat in the slots is generated distributed all over the windings.

- The slot shape – The slots are large, and in contact with the stator iron at many radii where the temperatures will be different, making it hard to model the paths through which the heat leaves. While the heat flow in e.g. the air gap can be approximated as radial and passing through all of the total resistance, the heat generated in the windings will leave the slots distributed over the entire surface of the slot/tooth surface and slot opening, and thus passing through an uncertain amount of thermal resistance.

First, lets have a look at how to find an approximation for the composite thermal conductivity of the slot material. It is not possible, nor desirable, to model every individual copper conductor. In [9], three ways of approximating the coppers conductance for lumped modelling are mentioned. A variation of one of them, composite thermal conductivity, is commonly used and is considered a suitable option. A DC-test is required to know it with

accuracy, but as that is not available, approximations based on other papers will have to serve. In [1] a variation of it is used, and a relation is suggested between the equivalent thermal conductivity of the slot mix and the stator slot fill-factor (i.e. the amount of copper in the slot). According to that relation, $\lambda_{sMix} \approx 2.5\lambda_{impreg} = 0.5$, which will be used for the contents of the slots in the FEM-model as well as the network model.

Surrounding the windings are the slot insulation and air pockets, which can be treated as two layers of film of thickness d_i and d_a respectively. The equivalent thickness of the air pocket layer d_a is difficult to find out, but it was in [1] estimated empirically to 0.17 mm for a 4 kW machine, and 0.3 mm for 15 kW machine. The d_a used in the simulations is therefore estimated to 0.235 mm. d_i on the other hand is given in Table 6 as 0.4 mm. The sum of the insulation thickness and the gap length is denoted d.

The chosen resistance calculation method is mostly based on the one presented in [1, pp. 59-63], with some lesser modifications. First we define an equivalent height h and width w of the slots by approximating the shape as a square, according to

$$h = h_{t3} + \frac{h_{t2}}{2} - 2d \tag{25}$$

and

$$w = \frac{A}{h + 2d} - 2d \tag{26}$$

where A is the total area of the slot. Based on these dimensions and the thermal conductivities of the materials in the slot, the following parameters are then calculated

$$R_{ix} = \frac{d_i}{h\lambda_i} + \frac{d_a}{h\lambda_a} \tag{27}$$

$$R_{iy} = \frac{d_i}{w\lambda_i} + \frac{d_a}{w\lambda_a} \tag{28}$$

$$R_{x0} = \frac{b}{h\lambda_{sMix}} \tag{29}$$

$$R_{y0} = \frac{h}{b\lambda_{sMix}} \tag{30}$$

$$R_x = 0.5\left(R_{ix} + \frac{R_{x0}}{6}\right) \tag{31}$$

$$R_y = 0.5\left(R_{iy} + \frac{R_{y0}}{6}\right) \tag{32}$$

All of these expressions refer to the resistance per unit length. The total resistance between the slot and the surrounding nodes is then equal to

$$R_s = \frac{R_x R_y}{no_s l (R_x + R_y)} \left(1 - \frac{R_{x0} R_{y0}}{720 R_x R_y} \right) \tag{33}$$

For a node connected to slot, the total resistance is scaled according to

$$R_{s-node} = R_s \frac{\Phi_{sTot}}{\Phi_{s-node}} \tag{34}$$

where Φ_{sTot} is the total slot circumference, and Φ_{s-node} is the length of the surface connecting the slot with the body in question. Using that equation, the list of resistances associated with the slot is as shown in Table 12. R_{s-tw} and R_{s-tmid} together replaces R_{s-t} for the complex network.

Table 12: The thermal resistances connecting the slots with their surrounding nodes.

Resistance	Equation	Connecting surface length
R_{s-t}	(34)	Φ_{s-t} (slot-tooth)
R_{s-y}	(34)	Φ_{s-y} (slot-yoke)
R_{s-a}	(34)	Φ_{s-a} (slot-air gap)
Complex network		
R_{s-tw}	(34)	Φ_{s-tw} (slot-tooth wing)
R_{s-tmid}	(34)	Φ_{s-tmid} (slot-tooth mid section)

The node placed in the slot represent the average temperature. There will be a rather strong temperature gradient in the windings, meaning that the maximum winding temperature can be a lot higher than that. It can be calculated from

$$T_{max} = T_a + (T_{av} - T_a) \frac{(R_{ix} + 0.25 R_{x0})(R_{iy} + 0.25 R_{y0})}{4 R_x R_y} \left(1 - \frac{R_{x0} R_{y0}}{384 R_x R_y} \right) \tag{35}$$

where T_a is the temperature of the ambient nodes.

3.3.5   Stator Teeth

For the teeth model, two different segmentations are used. These are shown in Figure 17, and the corresponding resistances in 13. As neither way of dividing the tooth is exclusive to radial/circumferential flows or the simple/complex model, they are all presented and named referring to the segment name only.
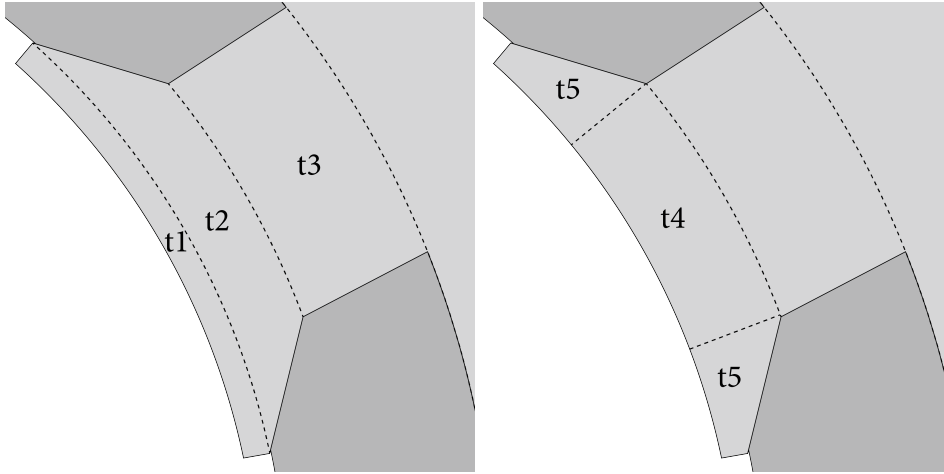
Figure 17: Two ways of dividing the teeth into segments for radial and circumferential resistance calculation.

Table 13: Thermal resistances in the teeth. // signifies a parallel circuit.

Resistance	Equation	Input				
		Inner radius	Outer radius	Angle	Inner width	Outer width
Radial direction						
R_{t1}	(16)	r_{t1}	r_{t2}	ϕ_{t1}		
R_{t2}	(14)	r_{t2}	r_{t3}		$\phi_{t2}r_{t2}$	$\phi_{t3}r_{t3}$
R_{t3}	(14)	r_{t3}	r_{t4}		$\phi_{t3}r_{t3}$	$\phi_{t4}r_{t4}$
R_{t4}	(16)	r_{t1}	r_{t3}	ϕ_{t3}		
R_{t5}		$\frac{2(R_{t4})(R_{t1}+R_{t2})}{(R_{t4})-(R_{t1}+R_{t2})}$				
Circumferential direction						
R_{t3-cf}	(18)	r_{t3}	r_{t4}	ϕ_{t3}		
R_{t4-cf}	(18)	r_{t1}	r_{t3}	ϕ_{t3}		
R_{t5-cf}	(18)	r_{t1}	$\frac{r_{t2}+r_{t3}}{2}$	$\frac{\phi_{t1}-\phi_{t3}}{2}$		
R_{t-cf}		$(2R_{t5-cf} + R_{t4-cf})//R_{t3-cf}$				

3.3.6   Yoke

The yoke is treated as a hollow cylinder. However, the temperature varies around the perimeter of the yoke rather noticeably, due to the different temperatures of the teeth and the slots. Rather than being calculated straight from (15), the yoke geometry can be divided into the segments shown in Figure 18 to be able to predict the heat flows from the inner nodes more accurately. Table 14 shows the thermal resistances for both networks.
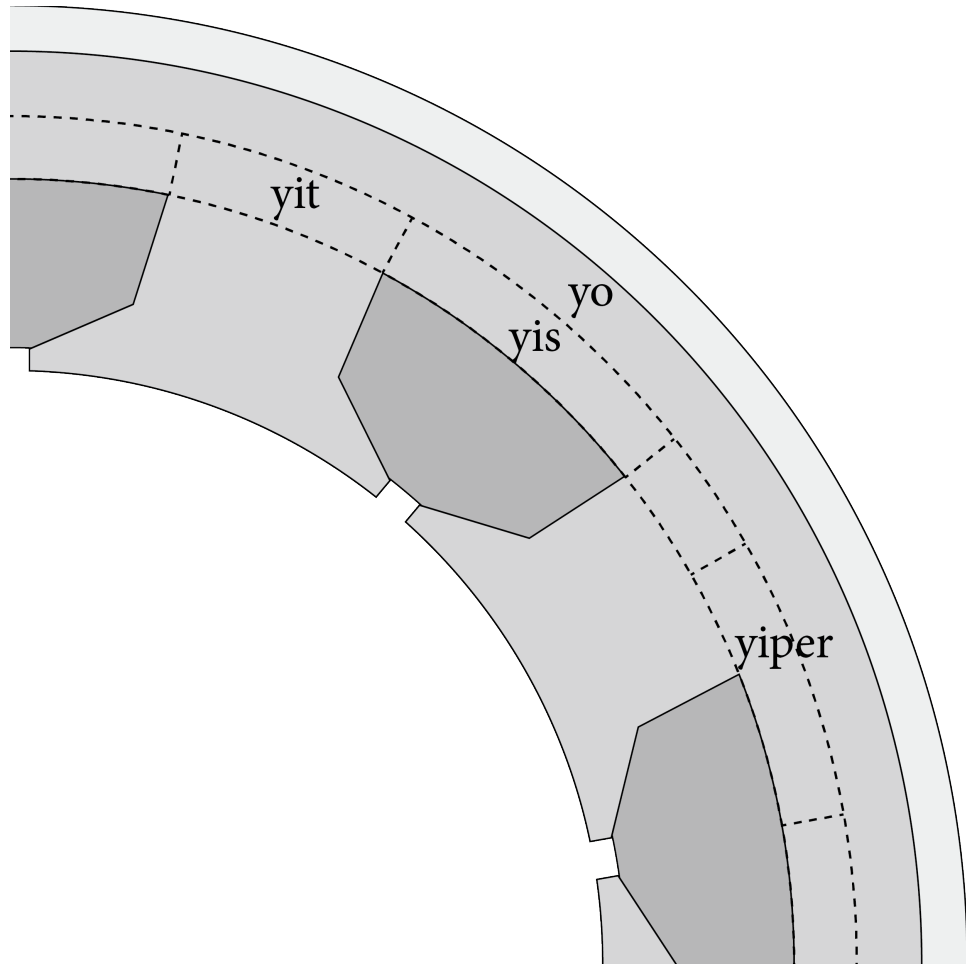
Figure 18: Dividing the yoke into segments for thermal resistance calculations.

Table 14: Thermal resistances in the yoke.

| Resistance | Equation | Input | | |
		Inner radius	Outer radius	Angle
Radial direction				
R_{yi}	(15)	r_{t4}	r_{yMid}	2π
R_{yis}	(16)	r_{t4}	r_{yMid}	ϕ_{s4}
R_{yit}	(16)	r_{t4}	r_{yMid}	ϕ_{t4}
R_{yo}	(15)	r_{yMid}	r_s	2π
Circumferential direction				
R_{yi-cf}	(18)	r_{t4}	r_{yMid}	$\frac{\phi_{s4}+\phi_{t4}}{2}$

3.3.7   Frame

The frame is modelled as a hollow cylinder. Its outer radius is that which corresponds to the average radius at which the cooling medium is in contact

with the frame. The resistance is presented in Table 15.

Table 15: Thermal resistance model for the frame

| Resistance | Equation | Input | | |
		Inner radius	Outer radius	Angle
Radial direction				
R_f	(15)	r_{sto}	r_{fo}	2π

3.3.8   Contact Resistances

In every situation where there are two objects that meet, there is likely to be a small air pocket separating them. Despite them being small, the fact that the thermal conductivity is much lower for air than for solids mean that they can not be neglected. This is modelled by estimating the average thickness of the air layer, and then calculating its resistance as conduction according to (4).

This was accounted for in [7, p.86], and has since been investigated more closely in more recent papers. The importance of good contact is stressed in [10]: *In addition, it requires a good thermal contact between the two surfaces in which heat transfer occurs. Without good thermal contacts, the use of expensive thermal conducting materials for the components is a waste.* In [9] there are tables with typical interface gaps lengths for several common materials used in electric machines.

In addition to the air pockets in between the stator iron and winding insulation described in Section 3.3.4, contact resistances are modelled for two places. The equivalent lengths of the interface gaps in the contact regions are based on data presented in [9, p.748]. For Al-Fe, an interval of typical interface gaps is given as 0.6-6 μm. For the stator-frame connection, 3.3 μm will therefore be used. For the magnets 10.2 μm will be used, which is the mean interface gap of Ceramic-Metal. The resulting resistances are then calculated according to Table 16.

Table 16: Expressions for the contact resistances

| Resistance | Equation | Input | | |
		Inner radius	Outer radius	Angle
$R_{contactf}$	(15)	r_{sto}	$r_{sto} + 3.3\mu m$	2π
		Width	Height	
$R_{contactm}$	(4)	w_m	10.2 μm	

3.3.9   Temperature Dependency

Increase in temperature has two major effects on the machine properties that will be taken into account in this paper. There is thermal expansion of metal, which will mainly affect the effective air gap length as described in 3.3.2. There is also the fact that the thermal conductivity generally is temperature dependent. For the materials where sufficient data has been available this have been attended to by iterating the solution and updating the thermal conductivity for each material from a lookup table.

3.3.10   Modelling Symmetries

The heat flows around the perimeter of the machine can generally be assumed to be symmetrical. That means that rather than putting a node on every single stator tooth, these symmetries can be used to scale the thermal resistance of every part to an equivalent thermal resistance. If there are x identical heat flow paths, x is the *symmetry factor*, meaning that the effective thermal resistance is only $1/x$ of that of a single element. For the rotor the symmetry factor around the magnets is no_m, and for the teeth and slots it is no_s.

For heat flows in the *circumferential* direction, the heat flows both clockwise and counterclockwise. If the thermal resistance between e.g. tooth node and slot node is calculated as the path between a single tooth and slot, that resistance should apart from the symmetry factor be further divided by a factor 2.

3.4   Node Connections in the Thermal Networks

The node configurations for the two thermal resistance networks were presented in 3.2. Here comes a brief presentation of how the nodes are connected, and what equivalent thermal resistances are said to represent those connections.

How the nodes are connected in the simple network is shown in Figure 19, while the equivalent thermal resistances for each connection is presented in Table 17. One difference from the networks in [1] and [7] is the addition of the connection between the slot and the yoke, rather than having all heat to leave the slots through the teeth node. That is an approximation that makes sense for the machines in those two publications, where there are more stator slots and most of their circumferences borders to the teeth. For this machine, the slots have a much wider shape, and the total slot resistance is thus distributed between the slot-tooth and slot-yoke connections.

For the complex network, the nodes are connected according to Figure 20 and the resistances are as specified in Table 18.
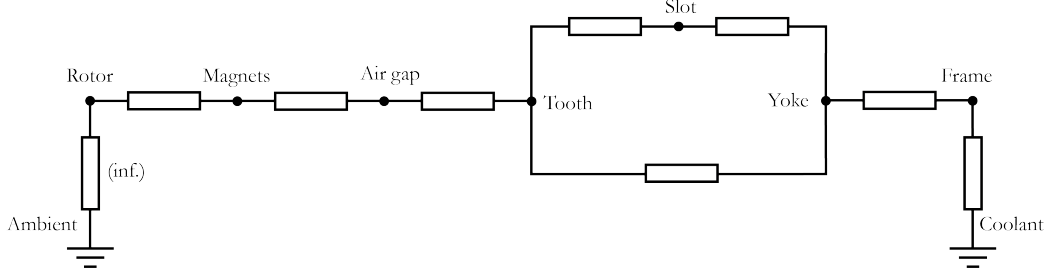
Figure 19: The connections for the simple thermal network.

Table 17: Thermal resistances connecting the nodes in the simple network.

Node 1	Node 2	Connecting Resistance	Typical Value [K/W]
Rotor	Magnets	$R_{rS1o} + (R_{contactm} + R_{rS2i}//\frac{R_{rS4}}{4})\frac{1}{no_m}$	$14 \cdot 10^{-3}$
Magnets	Air gap	$((R_{contactm} + R_{rS2o})//\frac{R_{rS4}}{4})\frac{1}{no_m} + R_{rS3} + R_g$	$350 \cdot 10^{-3}$
Air gap	Tooth	$(R_{t1} + R_{t2})\frac{1}{no_s}$	$5.6 \cdot 10^{-3}$
Slot	Tooth	$(R_{s-t}//R_{s-a} + \frac{R_{t-cf}}{4})\frac{1}{no_s}$	$190 \cdot 10^{-3}$
Slot	Yoke	$(R_{s-y} + R_{ysi})\frac{1}{no_s}$	$290 \cdot 10^{-3}$
Tooth	Yoke	$(R_{tS3} + R_{yti})\frac{1}{no_s}$	$16 \cdot 10^{-3}$
Yoke	Frame	$R_{yo} + R_{contactf} + \frac{R_f}{2}$	$3.2 \cdot 10^{-3}$
Frame	Coolant	$\frac{R_f}{2}$	$0.14 \cdot 10^{-3}$

When reading the expressions for the connecting resistances in the tables, many of the resistances referred to from Section 3.3 are divided by 2 or 4. That means that the node is placed in the middle of the geometry it represents and therefore only half of the distance will be covered, and/or there are two of the element in parallel for the heat flow to split up between. Division by a symmetry factor no_s or no_m means that the resistance is scaled because it only represents a fraction of the machine. // signifies a parallel circuit.

Table 18: Thermal resistances connecting the nodes in the complex network

Node 1	Node 2	Connecting Resistance	Typical Value [K/W]
n_r	no_m	$(R_{rC1o} + R_{contactm} + R_{rC2i})\frac{1}{no_m}$	$33 \cdot 10^{-3}$
n_r	n_{rs}	$\frac{R_{rC4}+R_{rC5}}{2}\frac{1}{no_m}$	$39 \cdot 10^{-3}$
no_m	n_{ms}	$(R_{rC2o} + R_{contactm} + R_{rC3})\frac{1}{no_m}$	$20 \cdot 10^{-3}$
n_{ms}	n_{rs}	$(\frac{R_{rC3-cf}}{4} + \frac{R_{rC6-cf}}{2})\frac{1}{no_m}$	$100 \cdot 10^{-3}$
n_{ms}	n_{ac}	$0.1R_g\frac{\phi_{rSym}}{\phi_m}$	$47 \cdot 10^{-3}$
n_{rs}	n_{ac}	$0.1R_g\frac{\phi_{rSym}}{\phi_{rSym}-\phi_m}$	$160 \cdot 10^{-3}$
n_{ac}	n_a	$0.9R_g$	$330 \cdot 10^{-3}$
n_a	n_{ti}	$\frac{R_{t4}}{2}\frac{1}{no_s}$	$4.4 \cdot 10^{-3}$
n_a	n_{tw}	$\frac{R_{t5}}{4}\frac{1}{no_s}$	$8.1 \cdot 10^{-3}$
n_a	n_{so}	$\frac{R_{sOpeningC}}{2}\frac{1}{no_s}$	$9100 \cdot 10^{-3}$
n_{ti}	n_{tw}	$(\frac{R_{t5-cf}}{4} + \frac{R_{t4-cf}}{4})\frac{1}{no_s}$	$19 \cdot 10^{-3}$
n_{so}	n_{tw}	$(\frac{R_{sOpeningC-cf}}{4} + \frac{R_{t5-cf}}{4})\frac{1}{no_s}$	$6400 \cdot 10^{-3}$
n_{ti}	n_t	$\frac{R_{t4}}{2}\frac{1}{no_s}$	$4.4 \cdot 10^{-3}$
n_{tw}	n_s	$R_{s-tw}\frac{1}{no_s}$	$400 \cdot 10^{-3}$
n_{so}	n_s	$(\frac{R_{sOpeningC}}{2} + R_{s-a})\frac{1}{no_s}$	$12000 \cdot 10^{-3}$
n_t	n_s	$(R_{s-tmid} + \frac{R_{t3-cf}}{4})\frac{1}{no_s}$	$390 \cdot 10^{-3}$
n_t	n_{yti}	$(R_{t3} + \frac{R_{yti}}{2})\frac{1}{no_s}$	$13 \cdot 10^{-3}$
n_s	n_{ysi}	$(R_{s-y} + \frac{R_{ysi}}{2})\frac{1}{no_s}$	$290 \cdot 10^{-3}$
n_{ysi}	n_{yti}	$\frac{R_{yi-cf}}{2}\frac{1}{no_s}$	$43 \cdot 10^{-3}$
n_{yti}	n_y	$\frac{R_{yti}}{2}\frac{1}{no_s}$	$2.7 \cdot 10^{-3}$
n_{ysi}	n_y	$\frac{R_{ysi}}{2}\frac{1}{no_s}$	$2 \cdot 10^{-3}$
n_y	n_f	$R_{yo} + R_{contactf} + \frac{R_f}{2}$	$3.2 \cdot 10^{-3}$
n_f	Coolant	$\frac{R_f}{2}$	$0.14 \cdot 10^{-3}$
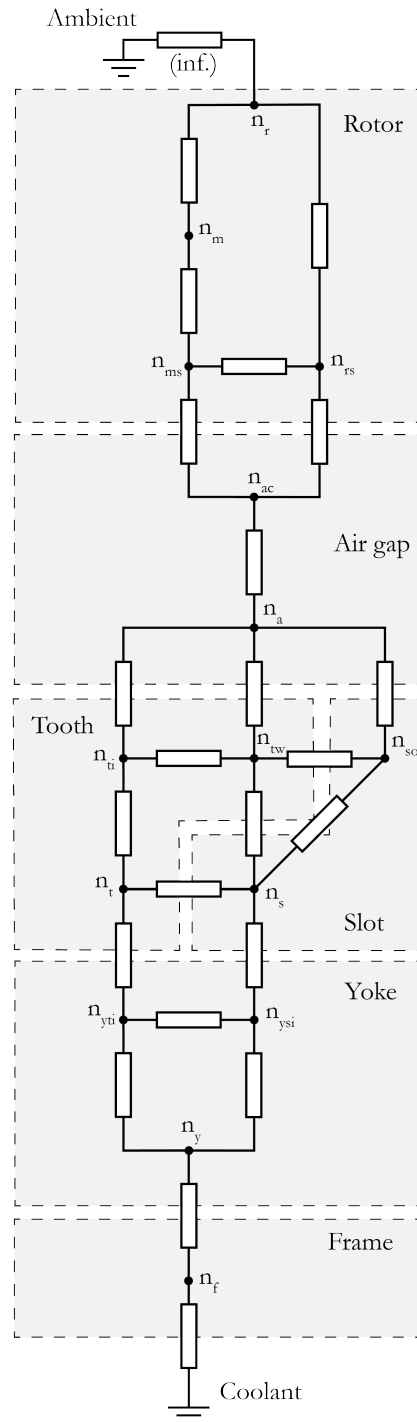
Figure 20: The connections for the complex thermal network.

3.5   FEM-Simulation

The settings of the FEM-simulation follows the principles described in this thesis, with a few exceptions. Some comments on how they were realised in ANSYS Mechanical are:

- The coolant was simulated by setting a constant temperature on the outer boundary of the frame.

- The reference temperatures used when comparing the FEM-simulation with the thermal network models are extracted by taking the temperatures of a small subelement placed at the exact location the network node would correspond to.

- To decrease the simulation time and make meshing easier, the machine is modelled as a 1 mm thin sheet.

- The mesh was refined to the extent that further refinement did not significantly alter the simulation result.

- Contact resistances are defined by setting the thermal conductance of the contact regions.

- The simulation of the slots assumes a material mix of the same thermal conductivity as for the thermal network.

- As Mechanical does not support simulation of gas and fluid movement, air is considered as solid. This can be partially handled by scaling the materials equivalent thermal conductance with the factor that would for the thermal network model be accounted for in the heat transfer coefficient. It does not however handle the fact that the air is constantly moving and roughly homogenous in its temperature distribution. As it does not, it means that hardly any heat will flow in the section of the air gap outside the slot openings, and ΔT over the air gap will hence essentially be overestimated by some amount.

3.6   Loss Input

Acquiring reliable loss estimations in electric machines without measurement data is a complex task. In the analysis of this report, the proposed loss magnitude and distribution is based on data from machines of similar size and type. It is intended to be plausible suggestions, without making claims of being the exact values for this particular motor. The loss distribution will be investigated in Section 4.3

Table 19 shows a comparison between three motors on which there are published papers including loss data. The first is Kylanders 4 kW induction machine [1], which can be of interest to compare with the others despite it having a caged rotor. The second is Lindströms PMSM [7], for which the

losses were measured through a calorimetric method and then separated and distributed according to a FEM simulation. The third motor is a HSPMG *(High Speed Permanent Magnet Generator)* presented by Li et al. [11].

Table 19: Estimated machine losses and related design parameters for machines similar to the PMSM studied

Parameter	Kylander	Lindström	Zhang	Investigated
Type	IM	PMSM	HSPMG	PMSM
Rated power [kW]	4	49	117	-
Rated speed [rpm]	1 435	6 000	60 000	-
Core length [mm]	105	231	275	200
Stator diameter [mm]	187.2	189	135	198
Volume estimation [dm^3]	0.92*	2.06*	1.25*	1.96*
Number of stator slots	36	48	36	9
Stator slot area [mm^2]	96	89.8	-	450.6
Stator slot fill factor	0.4*	0.45	-	0.45
Winding losses P_{Cu}[W]	390	822[1]	999	666*
Corresponding J [A/mm^2]	<12.5*	10.3*	-	10.3*
Core losses total P_{Fe} [W]	-	873*	1728	699*
– yoke	-	464 (53.1%)	1034 (59.8%)	358*(51.2%)
– teeth	-	387 (44.3%)	288 (16.7%)	271*(38.8%)
– rotor	-	22 (2.5%)	405 (23.4%)	70*(10%)
Windage & friction $P_{w}i$[W]	31	90	466	90

[1] Winding losses in coil sides only, excluding the end windings
* Calculated value, not given expressly
$^-$ No data

The volumes are estimated as those of cylinders of the same core length and stator diameter. They are provided to give an indication to the power density of each machine. The current density, J, gives an indication to the loading of the machine. It is calculated from the winding loss P_{Cu}, equivalent total copper area in all slots A_{Cu}, the axial length l and a copper resistivity $\rho_{Cu} = 1.72 \cdot 10^{-8}$ according to

$$J = \sqrt{\frac{P}{A_{Cu}l\rho_{Cu}}} \qquad (36)$$

Lindström states that while the total resistive losses are 1335 W for the machine, 822 W of those correspond the the losses originating in the coil

sides, i.e. the part of the windings "inside" the machine, excluding the end windings. Considering the fact that the end windings are usually the hottest part of the machine, there is likely to be some heat flow into that machine resulting in a slightly higher loss being dissipated radially through the stator. Kylander does not provide the same detailed information, and since equivalent end winding length is not known, the resulting current density for the IM machine can not be calculated. The upper limit however is 12.5, as that value would correspond having all 390 W generated in the coil sides.

The machine most similar to the one in this thesis is Lindströms PMSM. It is assumed that the loss distribution is rather alike, with the exception of the ratio P_{Fe_r}/P_{Fe_tot} being increased to 0.1 rather than 0.025, to be on the safe side. The core losses in the stator teeth and yoke appear to be proportional to their respective volumes, and so the heat generation in the stator will be modelled as uniform.

Having established a typical distribution of the iron and copper losses, the magnitude is then determined by looking at reasonable current density levels and by accounting for the machines thermal limits. The thermal limits are set depending on the specific materials in the machine and the desired safety margin, and are thus a topic for discussion. For the most sensitive parts, the magnets and windings, the limits are in [7] suggested as 100 and 130 degrees respectively. The current density can thereafter be set to emulate a load close to the thermal limits. An average steady state current density of 10.3 yields the data presented in Table 19.

The windage losses are proportional to ω^3 [12, p.19] and can in high speed machines make a considerable contribution to the total losses [5]. The correlation between speed and windage loss is also demonstrated by the machines compared, where the HSPMG displays much higher values than the others. $P_w i$ is as a consequence set to 90 W as the rated speeds are believed to be comparable between the two PMSM:s.

The nodes associated with each loss are shown in Table 20. In most of the cases there is not really any question of which node to assign them to. The exception is the windage and friction losses $P_w i$ which are lumped together and placed in the air gap. Also, as the distribution of the rotor core losses between the rotor iron and the magnets, they are assigned to the magnet node to adapt to a "worst case" approach.

Table 20: Loss assignment in the simple thermal network.

Node	Assigned loss
Magnets	P_{Fe_r}
Air gap	$P_w i$
Windings	P_{Cu}
Tooth	$P_{Fe\_st} \frac{V_t}{V_{st}}$
Yoke	$P_{Fe\_st} \frac{V_y}{V_{st}}$

4   Steady State Analysis

All analysis is made for steady state, meaning that the point of operation has remained constant long enough for all parameters and temperatures to stabilise. Furthermore, the coolant is assumed to retain a constant temperature of 22 degrees. For many applications the cooling will be less effective, which would mean that the temperature "offset" in the simulation would be higher, and consequently there would be less margin before the thermal limits are reached.

For many simulations, the results from both the network analysis and the FEM solution are presented. Care should be taken when comparing the temperatures. The network analysis gives a representation of the *node* temperatures, which usually corresponds to the average at that radii or body. The FEM values on the other hand are the exact values at a very specific point in the machine. The difference in the methods is not very large, but means that there is some level of arbitrariness in how the results are presented. Being able to see a conformity between the resistance network model and the FEM model still gives a useful indication towards the reliability of the network model.

Images of the temperature distribution and heat flux from the FEM-simulation have been included in Appendix A.

4.1   Comparison of Resistance Networks and FEM-Solution

The first simulation of the machine is done with all three solution methods presented in Section 3. The results are compared for the machine when it is run with all parameters set to their normal values. The idea is to see how much can be gained from increasing the resolution of the node configuration and discuss the credibility for the network that will be used throughout the simulations. Table 21 contains the output from the initial simulation and presents how well the FEM and the network solutions agree.

Despite the fact that FEM-solutions are potentially very accurate, they are in some ways subject to the same uncertainties in the input data as the network models. If there would for instance be an estimation error in the interface gap between two materials, it would yield the same error for both models. Also, the simplification of having a uniform heat generation goes for both ways of simulating. And when it comes to the simulation of the air gap, the network model is probably more reliable, as it handles the movement of air better than the FEM solution according to the reasoning in Section 3.5.

Looking at the yoke and the tooth node, the network temperatures are higher than the FEM solution. That is to be expected considering the conclusions drawn in Section 2.4.2, where it is concluded that the principle of

Table 21: Comparison of the simulation results from two thermal resistance network models and the FEM-simulation.

Node	FEM [$°C$]	Complex Network			Simple Network		
		T [$°C$]	ΔT	$\Delta T[\%]$	T [$°C$]	ΔT	$\Delta T[\%]$
Rotor	68.37	68.14	-0.23	-0.34	66.65	-1.73	-2.53
Magnet	68.76	68.70	-0.06	-0.09	66.65	-2.11	-3.07
RotorOFe	67.71	67.48	-0.23	-0.33			
RotorOMagnet	67.93	67.52	-0.42	-0.61			
RotorOConnection		64.94					
Airgap	[40.1,43.3][*]	41.84			40.45		
SlotOpening		56.88					
SlotAverage		107.31			104.75		
SlotMax	127.43	131.91	4.48	3.51	128.47	1.04	0.81
ToothWing	42.2	42.45					
Tooth	38.0	39.32	1.32	3.46	39.52	1.52	3.99
ToothOuter		40.77					
YokeInnerSlot	26.46	27.46	1.00	3.78			
YokeInnerTooth	29.33	28.92	-0.41	-1.41			
Yoke	26.8	26.85	0.04	0.16	26.85	0.04	0.16
Frame	22.19	22.20	0.01	0.05	22.20	0.01	0.05
Simulation time [s]	362	0.99			0.94		

[*] Highest and lowest temperature on corresponding surface

loss injection in a node will overestimate the temperature at that particular node. What is more important is perhaps that the estimation of the total temperature increase in the body is correct. The air gap node is placed on the boundary between the teeth and the air gap, and is thus determined by the modelling of the teeth and not of the air gap itself. That the air gap temperature agrees rather well between the models is hence a better indication to whether the stator models are in accordance than comparing the teeth node.

The high resolution thermal network appear to give a more accurate temperature prediction than the low resolution network of the stator iron. For the slot node however, it is actually the simple networks that agrees the best with the FEM solution. That is probably due to the fact that the complex network models the slot openings, meaning that a fraction of the slot conductance is coupled with high resistance node rather than the tooth node. The latter is the case for the simple network, but of course would the heat transfer from the slots be improved if it was actually all surrounded by iron rather than air. The improvement in the slot temperature estima-

tion for the simple network can thus probably be explained by two errors of opposite signs cancelling each other out.

Whether all additions in the complex network are worth the extra effort and complications can be discussed. Starting by considering the extra nodes in the rotor, they change the magnet node temperature with 0.7 degrees compared to the simple network. For the yoke, introducing the same two extra nodes from the complex model to the simple model had very little effect; only 0.1 degrees lower temperature in tooth, rotor and magnet node, while the slot node was unaffected. If only one of the additions in the complex network were implemented that should be the more detailed simulation of the teeth, which affects the temperature of the air gap and rotor nodes with 1.3 degrees. Due to the shape of the slots, the effect of the heat flowing from the inner path of the slots and through the entire teeth rather than just out through the yoke is rather considerable.

The complex network is what is used for most of the upcoming simulations.

4.2 Sensitivity Analysis
A comprehensive sensitivity analysis can give an indication to which parameters are important to the simulated temperatures. Therefore a number of parameters of interest are swept to thereby get an idea of which to take a closer look upon.

4.2.1 Overview of Selected Parameters
For the second sensitivity analysis shown in Table 22, a number of machine parameters have been selected and swept. They have been chosen because the data is either uncertain, or simply having a significant impact on the result. How much they are altered depends on the reasonable intervals they are likely to vary. Contact gaps for instance may vary greatly between different alloys but also between individual machines, whereas the width of the magnets is not prone to change much as it is mostly determined by the electromagnetic demands of the designer. The most interesting parameters are later on investigated in more detail in this section.

Table 22: Sensitivity analysis – Importance of selected parameters

	Change (%)	Value	Rotor	Magnet	Air gap	Slot max	Tooth	Yoke
					Node Temperature [$^\circ C$]			
No Change			68.14	68.7	41.84	131.91	39.32	26.85
Design Parameters								
h_g	-50	0.35 mm	55.26	55.82	42.01	132.31	39.49	26.92
h_g	$+100$	1.4 mm	69.19	69.75	41.52	130.69	39.01	26.7
w_{Magnet}	-24	25 mm	68.15	68.95	41.84	131.91	39.32	26.85
w_{Magnet}	$+21$	40 mm	68.17	68.59	41.84	131.91	39.32	26.85
h_{Magnet}	-50	2.5 mm	68.08	68.59	41.84	131.91	39.32	26.85
h_{Magnet}	$+100$	10 mm	68.25	68.91	41.84	131.91	39.32	26.85
$h_{minRotFe}$	-50	0.5 mm	68.13	68.7	41.84	131.91	39.32	26.85
$h_{minRotFe}$	$+200$	3 mm	68.18	68.72	41.84	131.91	39.32	26.85
$h_{slotInsulation}$	-50	0.2 mm	68.1	68.66	41.79	126.38	39.28	26.85
$h_{slotInsulation}$	$+100$	0.8 mm	68.22	68.78	41.92	143.3	39.38	26.85
h_{Frame}	-50	3.5 mm	67.96	68.52	41.64	131.71	39.12	26.65
h_{Frame}	$+100$	14 mm	68.48	69.04	42.21	132.28	39.7	27.22
speed		1000 rpm	68.14	68.7	41.84	131.91	39.32	26.85
speed		3000 rpm	59.89	60.45	41.86	131.67	39.33	26.85
Uncertain Parameters								
cg_{frame}	-80	0.66 μm	67.0	67.56	40.58	130.65	38.06	25.59
cg_{frame}	$+400$	16.5 μm	73.85	74.41	48.12	138.19	45.6	33.13
cg_{magnet}	-80	2.09 μm	67.94	68.3	41.84	131.91	39.32	26.85
cg_{magnet}	$+400$	51 μm	68.77	70.51	41.84	131.91	39.32	26.85
cg_{slot}	-50	117 μm	67.93	68.49	41.6	108.62	39.14	26.85
cg_{slot}	$+100$	470 μm	68.36	68.92	42.07	175.21	39.5	26.85
$\lambda_{airSlotOp.}$	$+100$	$2 \cdot \lambda_{airgap}$	69.37	69.93	41.87	131.44	39.34	26.85
$\lambda_{airSlotOp.}$	$+400$	$5 \cdot \lambda_{airgap}$	69.43	69.99	41.93	130.64	39.37	26.85
Temp dep.	On		68.14	68.7	41.84	131.91	39.32	26.85
Temp dep.	Off		69.84	70.40	41.83	131.93	39.32	26.85
Materials								
λ_{Fe}	-20	22.4	72.1	72.69	46.13	135.12	43.02	27.57
λ_{Fe}	$+50$	42	62.77	63.3	36.01	127.56	34.3	25.89
$\lambda_{WindingMix}$	-80	0.1	68.46	69.02	42.19	262.95	39.58	26.85
$\lambda_{WindingMix}$	$+250$	1.75	67.98	68.54	41.66	99.19	39.18	26.85
λ_{Mylar}	-50	0.1	68.2	68.76	41.9	141.3	39.37	26.85
λ_{Mylar}	$+100$	0,4	68.11	68.67	41.8	127.1	39.29	26.85
$\lambda_{Magnets}$	-50	4.5	68.29	69.04	41.84	131.91	39.32	26.85
$\lambda_{Magnets}$	$+100$	18	68.06	68.53	41.84	131.91	39.32	26.85

4.2.2 Network Connections

One important concept is that it is not only the magnitude or the uncertainty of the resistances that matters. Their location in the motor can also be of importance. Since the heat mostly flows radially out towards the frame and is built up along the way by the addition of more losses, the same resistance placed in the centre of the machine is of less consequence of the overall temperature than if it belonged to a part close to the frame.

This can be seen in Appendix B.2, where all node connection resistances in the simple resistance network for the simple network are changed up and down. Altering them by the same amount is helpful for understanding how sensitive the model machine model is to e.g. a small design change. For a closer look at the certain network connections, Table 26 in the appendix can be closer studied.

4.2.3 Sensitivity to Loss Distribution

The losses are naturally very important to the temperature in the machine, and are highly dependent of the loading. High speeds for instance increase the windage and the iron losses, while the copper losses are proportional to the torque. In Table 23 three parameters are swept one at a time to get an idea of how the temperatures might vary between different operation points of the machine.

Table 23: Sensitivity to loss parameters.

Sweep value	Rotor	Magnet	Air gap	Slot max	Tooth	Yoke
			Node Temperature [$°C$]			
Sweeping P_{tot}, ordinary distribution						
1000	56.64	57.05	37.12	102.59	35.09	25.62
1300	65.98	66.52	40.94	126.36	38.52	26.62
1600	75.18	75.83	44.77	150.13	41.95	27.61
Sweeping P_{Fe}/P_{Cu} ratio						
0.4	70.35	70.96	41.64	121.05	39.2	26.85
0.45	68.14	68.7	41.84	131.91	39.32	26.85
0.5	65.94	66.44	42.04	142.76	39.43	26.85
Sweeping P_{stFe}/P_{rFe} ratio						
0.95	54.4	54.68	41.21	131.62	39.0	26.85
0.9	68.14	68.7	41.84	131.91	39.32	26.85
0.85	81.83	82.67	42.46	132.2	39.64	26.85

The first loss parameter is the magnitude of the losses. Given a constant distribution, it can be seen that the predicted node temperatures are linearly dependent of the loss level. Apart from determining the maximum average steady state power level of the motor, it is thus of little interest to further inquire that parameter.

More interesting to investigate closer is what happens when the location of the losses is changed. This has a noticeable effect on the temperature distribution in the machine, and will therefore be investigated in more detail in Section 4.3.

4.3 Loss Distribution

Based on the preliminary results in Section 4.2.3, the distribution of the losses between rotor and stator, respectively copper losses and iron losses is investigated more closely.

Figure 21 shows what happens when a larger proportion of the losses occur in the windings rather than the core. The impact on the winding temperature is rather considerable, while the magnet temperature decreases at a lower rate. This shows that the winding temperature is more sensitive to the losses than the iron.
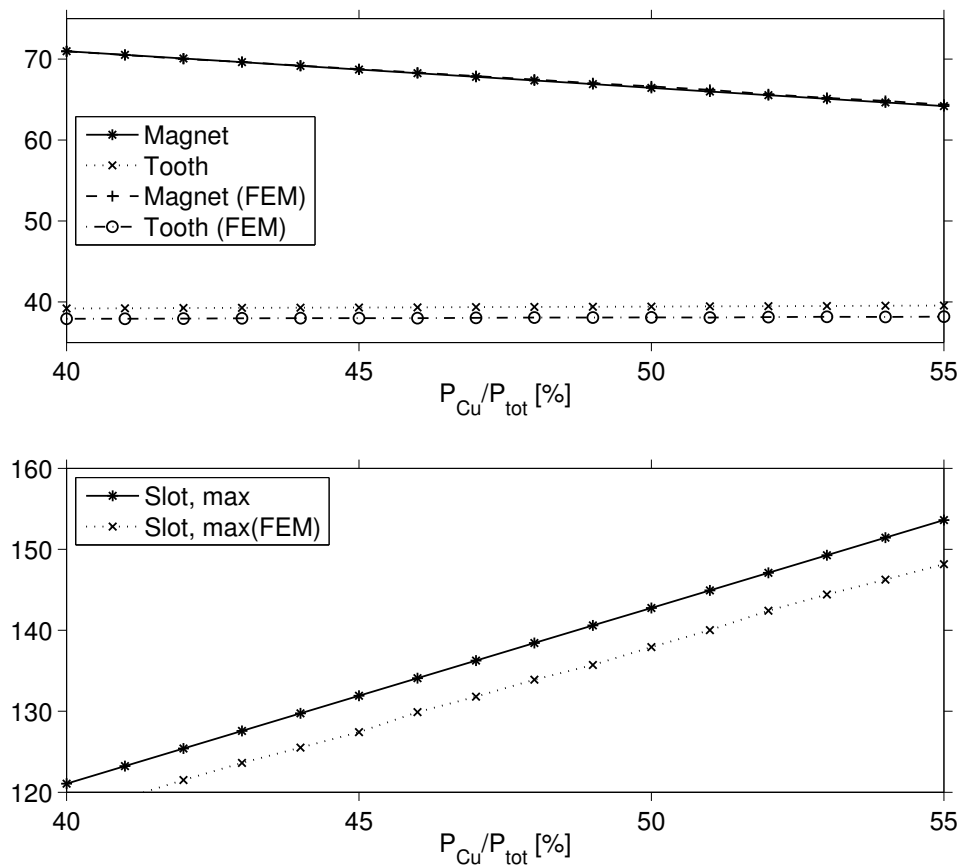

Figure 21: The effect of how much of the losses arise in the iron compared to the windings. The ambient temperature is 22 °C.

Figure 22 on the other hand shows the proportion of the iron losses that arise in the rotor, which turns out to have a considerable importance for the rotor temperature. The main reason is the high thermal resistance presented by the air gap. Although the loss distribution for this particular machine is not known, it is possible that the interval being swept, 0-20% of the core losses placed in the rotor, is very wide. The machine presented in [7] was declared to have around 2.5% core losses in the rotor, so it is likely that the left side of the plot in Figure 22 is the most relevant part. Not shown in the figure is the stator temperatures, which also increase marginally as the losses move to the rotor. It can thus be concluded that it is much easier to dissipate losses occurring in the stator than in the rotor.

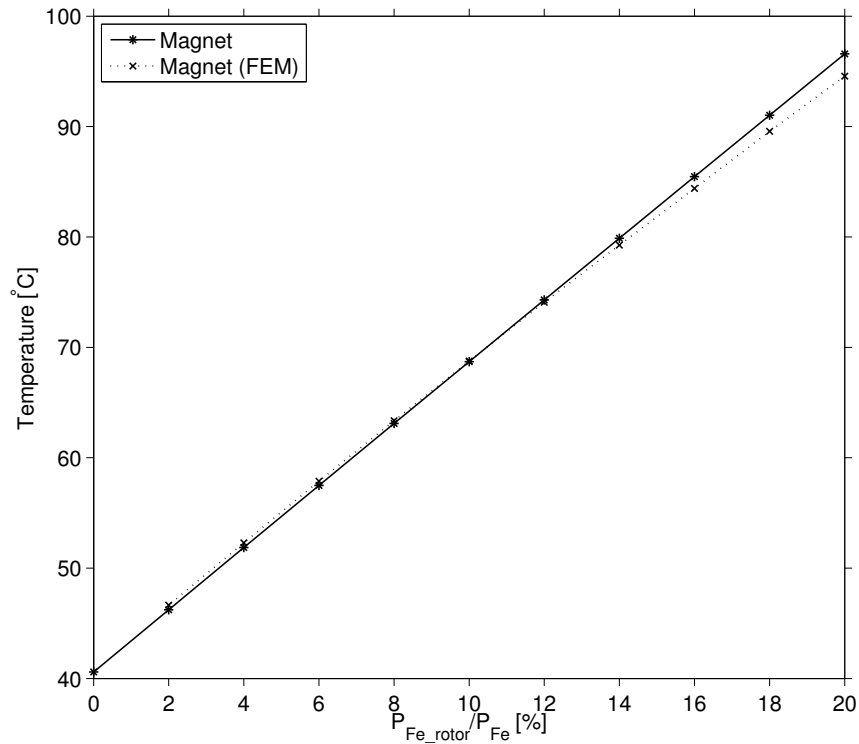Figure 22: The effect on the magnet temperature when sweeping the amount of the iron losses that is assigned to the rotor. The increase in the stator nodes is marginal. The ambient temperature is 22 °C.

4.4   Selected Machine Parameters

From the sensitivity analysis presented in Table 22, a selection of the most significant or otherwise interesting parameters are chosen to have a closer look upon.

4.4.1   Thermal Conductivity of the Iron Core

There is a wide variety of electrical steels available for using in motors. Rather naturally, the thermal conductivity of these may vary some. There is a negative correlation between the speed ratings of the machine and the thermal characteristics of the steel, as high speeds puts demand on good electrical insulation in the axial direction to keep Fe-losses down, which in turn unfortunately tend to have a negative impact on the thermal properties in the radial direction.

The thermal conductivity of the core material is of importance since most of the generated heat needs to pass through it. Figure 23 shows the dependency for the temperature of the core material. The temperature increase when lowering the thermal conductivity is roughly similar for most nodes. The magnitude of the change is roughly 10 degrees for λFe changing from 22 to 42 W/mk. The thermal conductivity of the core material is not unimportant, but compromising other properties of the core material to improve the thermal behaviour slightly is not likely to be a very effective solution.
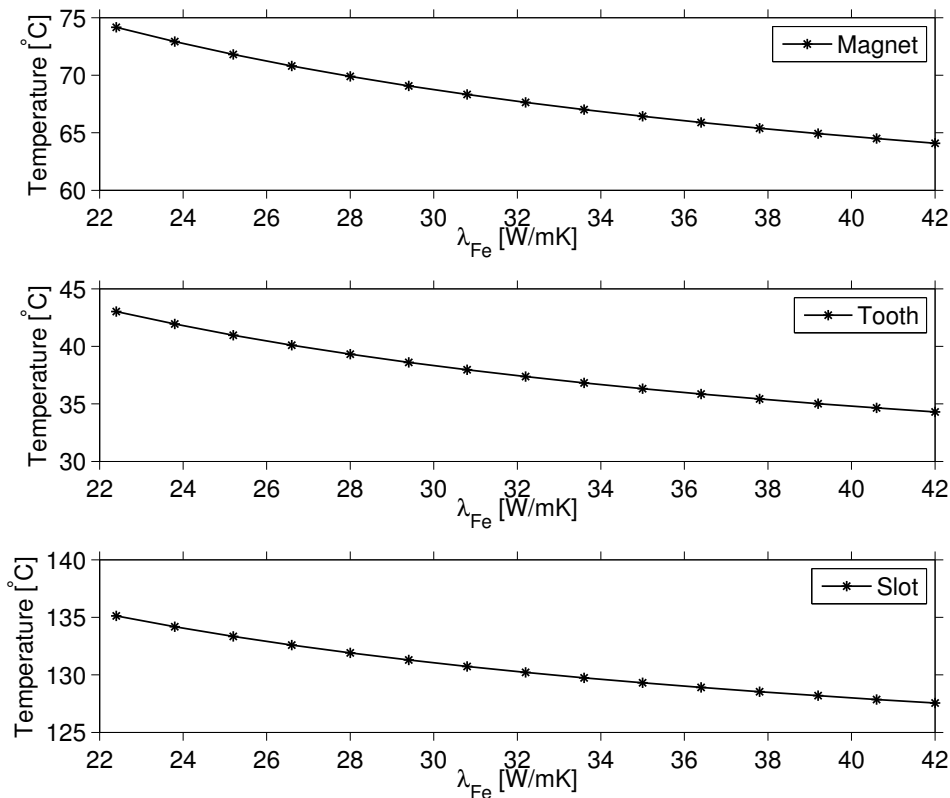
Figure 23: The importance of the equivalent thermal conductivity for the Fe-lamination mix for a few important nodes. The ambient temperature is 22 °C.

4.4.2   Equivalent Thermal Conductivity for the Winding Mix

The stator slots present one of the most challenging and uncertain aspects of modelling an electric machine. Some of the uncertainty arise from the fact that there are numerous ways the winding can be done and that different materials could be used to keep the windings steady and improve its thermal properties.

In this paper, the equivalent thermal conductivity for the winding mix in the radial direction is set to 0.5 W/mK. Figure 24 shows how the slot temperature depend on that parameter. As can be seen in the figure, basically the machine part affected by this change are the windings themselves. The results when lowering λ_{sMix} further below 0.5 is striking, which highlights the importance of the the windings when considering the thermal characteristics of the machine.
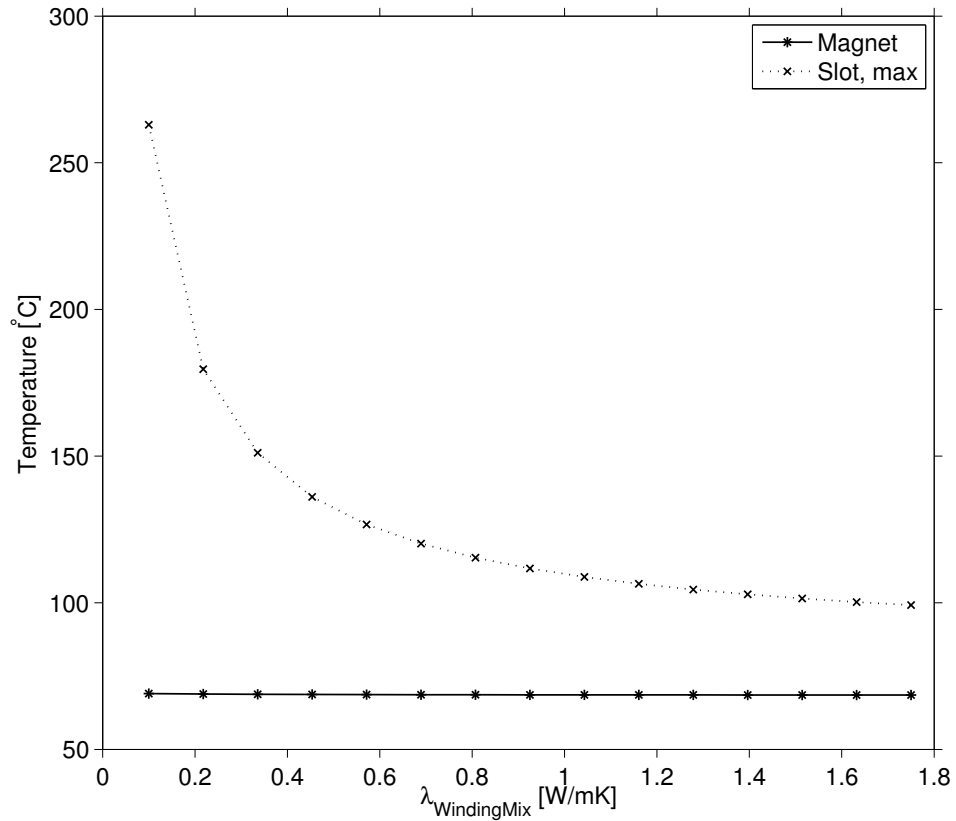
Figure 24: Sweeping the equivalent thermal resistance of the winding mix in the slots. The ambient temperature is 22 °C.

4.4.3 Contact Resistances

The contact gaps between components in the motor is impossible to know for certain. Based on data presented in Section 3 the contact gap between the stator and frame is set to 3.3 μm, but could for Al-Fe connections be both considerably higher or lower. Figure 25 shows how the machine temperatures would vary accordingly. Only the yoke node is shown, all nodes are altered by the same amount.
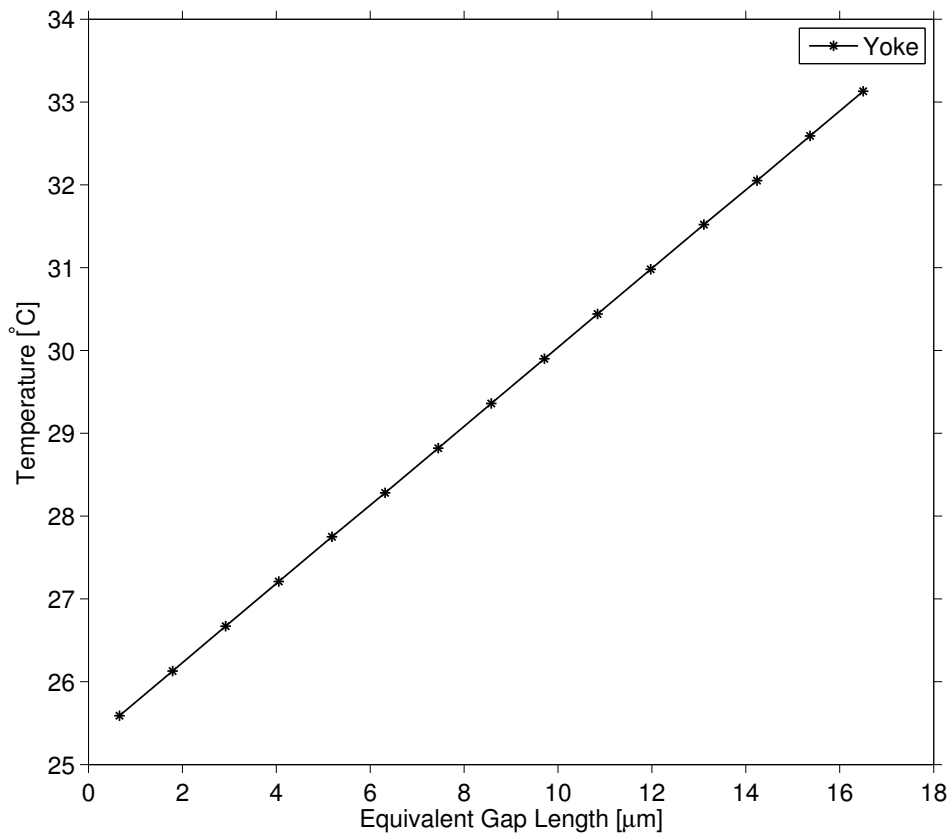
Figure 25: Sweeping the interface gap between the stator iron frame aluminium. The ambient temperature is 22 °C.

Figure 26 shows a similar sweep made for the interface gap between the winding insulation and the stator. The effect it has on the winding temperature is very pronounced as an increase from the lower to the upper limits of the "reasonable interval" would cause as much as a 66 degree increase, from solely the interface gap. The temperature in the rest of the motor is largely unaffected, the rotor only noticing a 0.5 degree increase for the same interval.
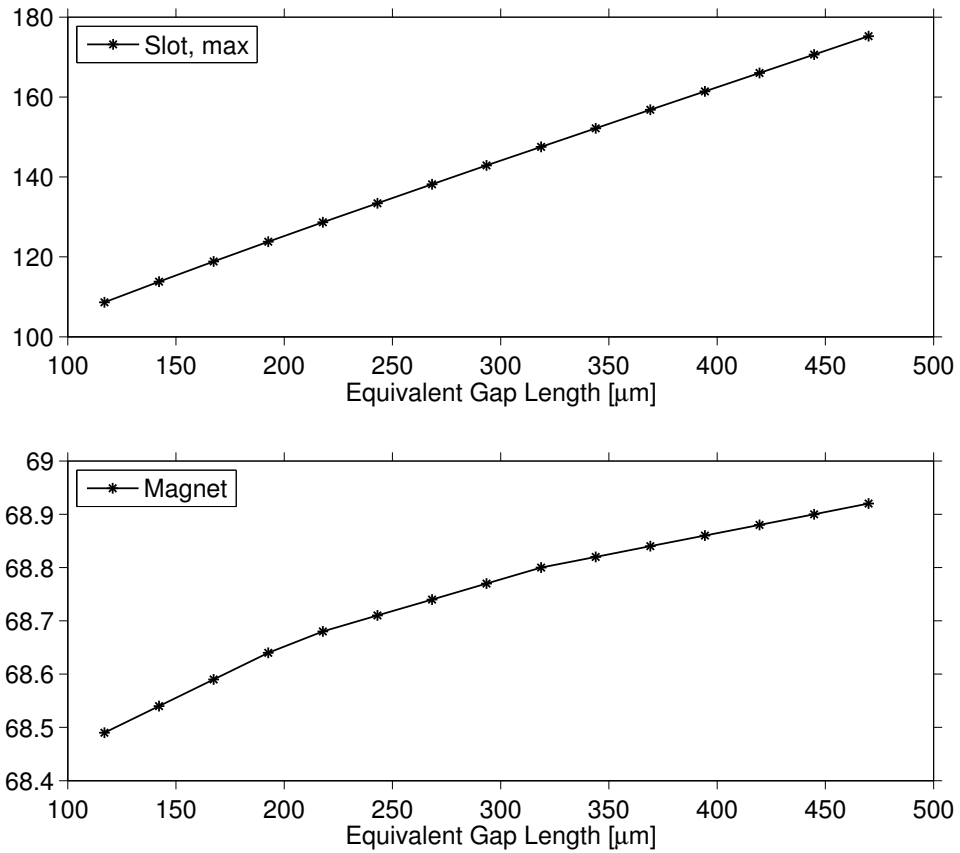
Figure 26: Sweeping the interface gap between the stator iron and winding insulation. Pay attention to the different scales on the subplots. The ambient temperature is 22 °C.

4.4.4 Air Gap

Due to the high thermal resistance of air, the air gap poses a strong barrier to the heat generated in the rotor. The convective heat transfer due to the movement of the air is difficult to model accurately, as there is a lot of uncertainty around the turbulence which has a positive impact on the heat transfer. Furthermore there is the thermal expansion of the rotor to consider.

Two parameters that affect the rotor temperature will be investigated. First off, the speed of the motor is very important for the turbulence in the air gap. Figure 27 shows how the speed impacts the rotor temperature according to the turbulence model in Section 3.3.2. There is a threshold at 1700 rpm before which the flow is considered laminar. Thereafter Nusselts number starts to increase and thereby impact the rotor temperature.
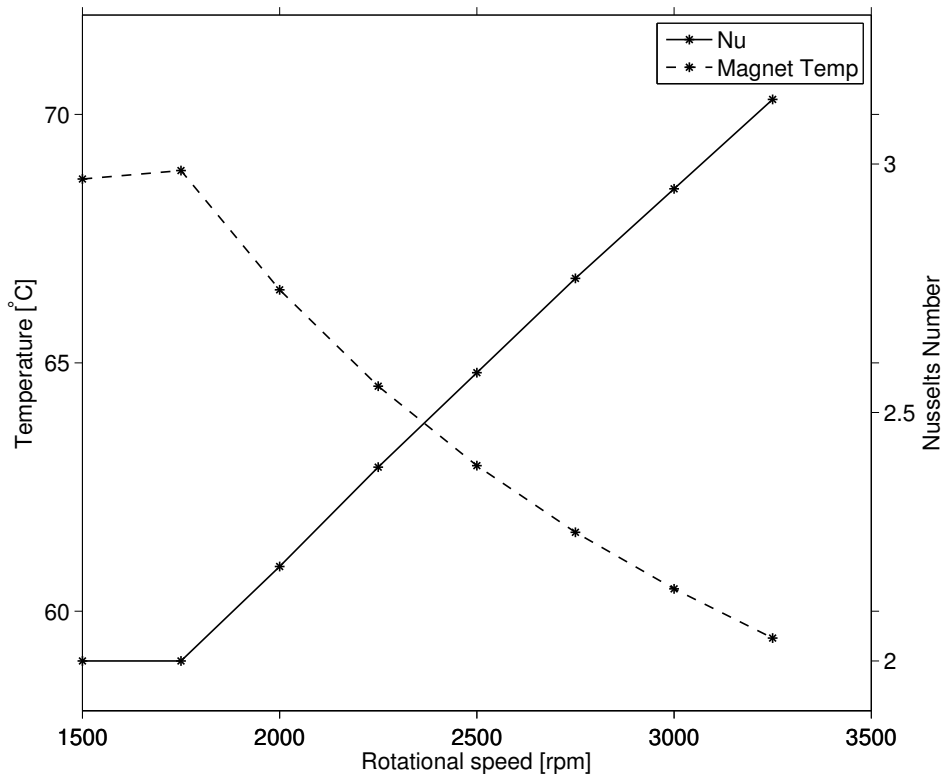
Figure 27: Sweeping the rotational speed. The ambient temperature is 22 °C.

Secondly, there is the rotor temperature itself, which affects the thermal conductivity of the air. It also makes the rotor iron expand, thereby decreasing the gap length. This in turn has two consequences. If the rotor expands, the heat needs to pass a shorter distance of air, but at the same time the air flow will turn a bit more laminar. The effect the gap length has on the predicted rotor temperature can be seen in Figure 28. The first curve shows the relation if the turbulence is assumed to be negligible, compared to if the machine runs at a speed of 1500 rpm and uses the turbulence model.

The turbulence model is one of the more uncertain aspects of the model, for which reason the specific temperatures given in the plots are not sure to be accurate. The influence it has is substantial however, and it points out that the heat transfer from the rotor is not necessarily proportional to the air gap length. The model is approximative, but it is with all likelihood better to include it than not doing so.
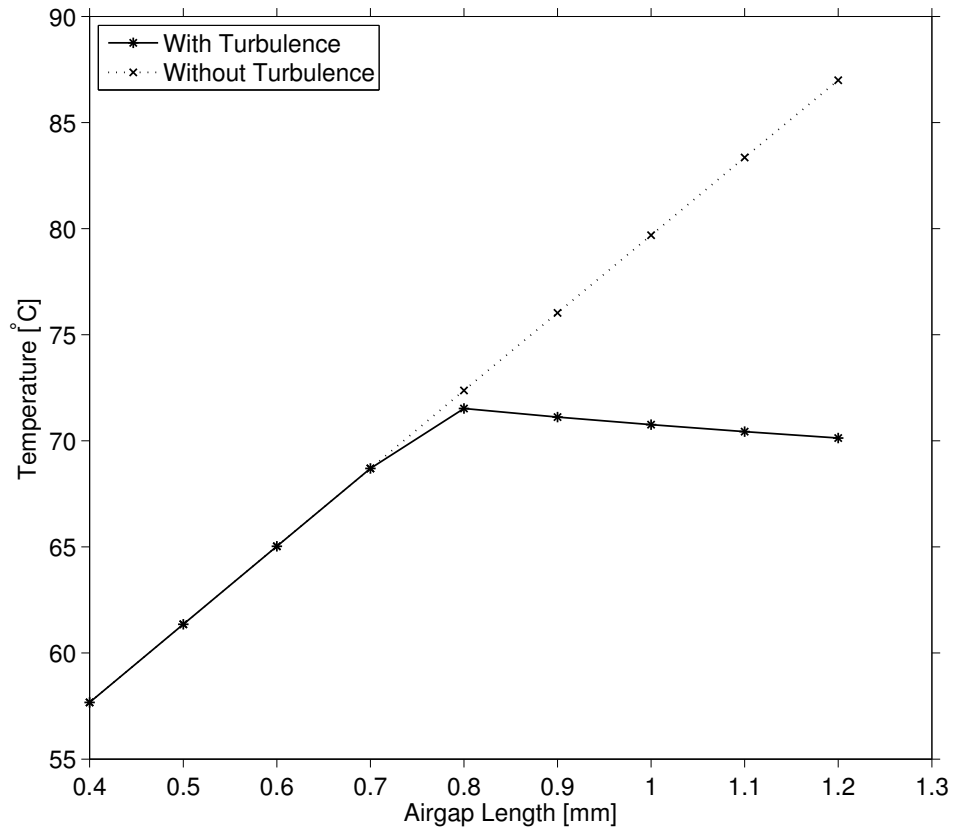
Figure 28: The magnet temperature for different air gap lengths – with and without accounting for turbulence. The ambient temperature is 22 °C.

4.5   Node Placement in the Teeth

In Section 2.3.2 the importance of the exact radial location of a node in a cylindrical object with internal heat generation is investigated. Now, a similar research is done but specifically the tooth node, with the rest of the surrounding network in place. The analysis is based on the simple node configuration, as the low number of thermal resistances affected by the node location made it more practical to sweep.

Figure 29 shows what happens if the machine geometries remain constant but the injection point is varied between different radii in the teeth. $r_{inj} = 0.63$ corresponds to all the losses arising on the teeth-air gap surface and passing through the entire teeth, while $r_{inj} = 0.79$ means the opposite. The temperature difference between the two extremes correspond to roughly $6°C$. The figure shows the node temperature of the air gap node and the magnet node, as those account for the total influence of the teeth modelling. Since the tooth node both moves, and according to Section 2.4.2 does not correspond well to the temperature at that a specific radius anyway, comparing

that with the FEM solution is not very meaningful. What matters is essentially the slope of the air gap and the magnet nodes, which shows the actual effect it has on the network. The inner nodes such as the magnets are all affected by the same amount, while nodes close to the frame are unaffected.

Figure 29: The influence of the radial location where the tooth node losses are injected. The ambient temperature is 22 °C.

5   Conclusions

This thesis has investigated the thermal behaviour of a PMSM. Besides getting an actual temperature prediction of the machine in question, it has been possible to point out a number of general observations regarding uncertainties in the input data, important aspects when setting up therm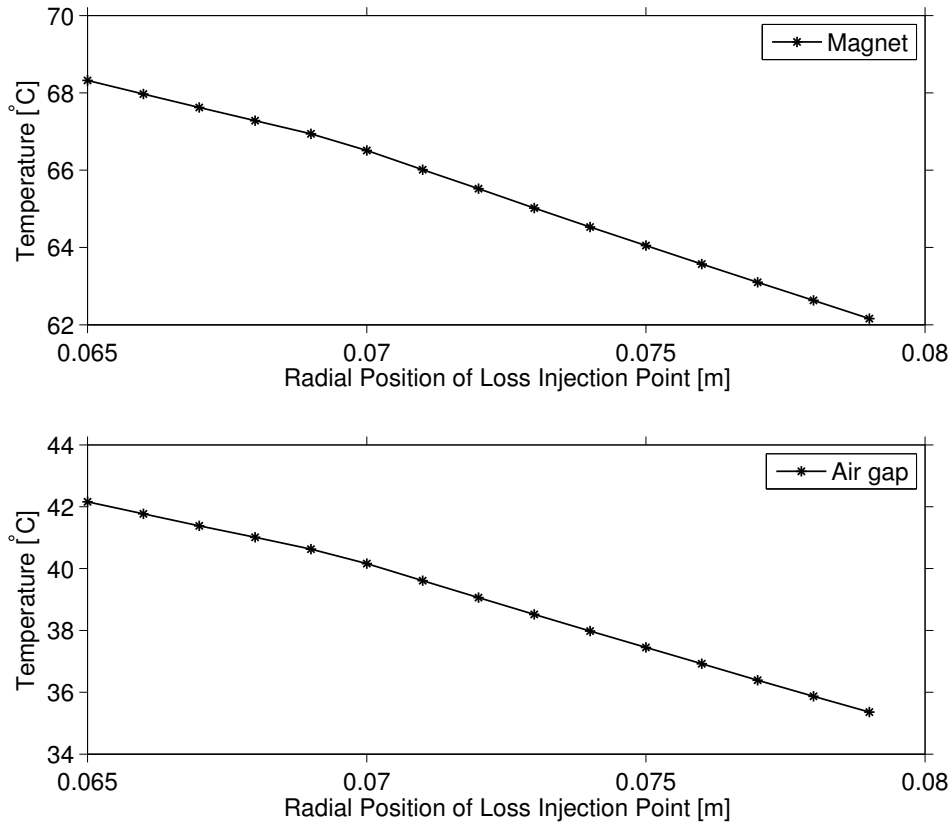al resistance network models, and what machine parameters should be considered for their thermal properties already in the design stage.

Thermal modelling, as all kinds of modelling, is intrinsically uncertain. Even with a lot of time and resources to perform careful measurements it can be difficult to obtain accurate estimations for some parameters. In this thesis, all such measurements have been replaced by basing basing data on other, more or less similar machines. However, motors naturally differ between different designs, and sometimes even noticeably between individuals of the same design. Furthermore, there are the limitations to the model to consider, such as the fact that axial heat flows and temperature gradients are not investigated.

This uncertainty goes for the analytical network model as well as for the FEM-model. While the latter might be more accurate in some ways, it is still subject to the same errors in the input data and limitation to the which phenomena is modelled. The FEM-solution can hence not be considered as the correct solution the way that actual temperature measurements on the machine could. The exact numbers presented in this investigation should therefore not be regarded as the important part of the result. What is more interesting is perhaps the comprehensive presentation of the thermal behaviour of an electric machine, and identification of the importance of several major parameters.

The most important machine part to pay attention to, both when modelling and designing a motor, is probably the windings. To begin with, simulations show that the windings are the part that first begins to take damage and thereby sets the limits of the maximum power output. Secondly, the temperature there depends on many factors that the designer could influence. For instance there is the choice of impregnation and insulation materials, maximising the slot fill factor, using a filling material in the slots with good thermal properties, and during the machine assembly trying to minimise the interface gaps. Thirdly, these parameters are difficult to estimate, and therefore constitutes a considerable source of uncertainty in the model.

The second part of the machine with a large importance for both the accuracy of the modelling and the thermal behaviour of the machine is the air gap. The major source of uncertainty when modelling it is the turbulence of the air, which require CFD simulations, and the thermal expansion of

the rotor. Since the thermal resistance of air is very high, the air gap has a considerable impact on the rotor temperature and makes it very sensitive to increase in the rotor losses.

Another thing that can be of interest to consider is the interface gap between the stator iron and the frame. Though not as significant as the gap around the windings, the fact that it is placed close to the boundary of the machine means that it produce an offset affecting basically all the machine. By being aware of that when the machine is manufactured, unnecessarily large gaps can perhaps be avoided.

Apart from investigations regarding the different aspects of the machine, some general methods for thermal network modelling have been reviewed. One was the possibility of the improving the accuracy of the network by increasing the resolution of the node configuration. The result was quite ambiguous. On one hand, the temperature estimation in some machine parts seems to be improved some by the addition of some extra nodes in the stator and rotor iron. The exception is the slot node, although it can not be said whether this is due to additions of the nodes, or because slot-tooth conductance is overestimated by some other simplifications in the low resolution network.

A major difference between the two networks is the complexity. More nodes means more node connections, and the resistances of smaller machine segments often turn out less "natural" to calculate and the necessary simplifications more difficult to justify. The conclusions is thus that using a more high resolution node configuration solely to improve accuracy is in itself not worth the effort, and the conventional node configuration is good enough for most application unless the increase in resolution itself is something that is desired.

Investigating the results of different resistance calculation methods for slightly more complex geometries, such as the teeth, did not yield entirely clear results neither. For simple shapes with well defined heat flow paths, the analytical ways of calculating the thermal resistance can be very accurate. For more complex shapes where the heat paths can vary more, the solutions tend to be more approximative. For the teeth segments in this machine, (14) turned out to be the best equation to use, but that can not be generalised to other machines and shapes.

One experiment where the outcome turned out in favour of the proposed method was when investigating the loss injection points in the model of a machine part with a distributed heat generation. Rather than for the sake of simplicity placing a node with half the resistance on either side, its placement should be chosen with respect to both the accumulated resistance and volume of a geometry in direction of the heat flow. For shapes similar

to hollow cylinders, such as is the case with the stator yoke for instance, the results were improved by calculating the resistance on the inside and the outside of the radial mid point of the cylinder.

5.1   Future Work

The thermal models presented covers most aspects of the electric motor that is modelled, but naturally there are things that can be further developed. The most obvious is the addition of the axial flows. That essentially means adding nodes for the end windings, the internal air, and perhaps the bearings. The choice of cooling method is another thing that could be relevant to investigate. Additionally, the thermal mass could be included in the modelling to enable performing transient simulations in addition to steady state operation.

At the time of writing, the investigated machine has just recently become available, and temperature measurements will soon take place. This could help to identify any weak spots in the modelling. Further tests on the motor could also improve the input data used in the simulation. The losses are the inputs that could be improved the most, which could be done through a combination of actual measurements and electromagnetic simulations in ANSYS Maxwell.

References

[1] G. Kylander. "Thermal Modelling of small cage induction motors". PhD thesis. Chalmers University of Technology, 1995.

[2] K&K Associates. *Thermal Network Modeling Handbook*. Version 97.003. Nation Aeronautics and Space Administration. 1976.

[3] M. Kaufman. *Principles of Thermodynamics*. CRC Press, 2002. ISBN: 978-0-203-90976-8.

[4] Zhang. *Radiative Transfer Through Transparent Media*. July 2010. URL: https://www.thermalfluidscentral.org.

[5] J. Nerg, M. Rilla, and J. Pyrhonen. "Thermal Analysis of Radial-Flux Electrical Machines With a High Power Density". In: *Industrial Electronics, IEEE Transactions on* 55.10 (2008), pp. 3543 –3554. ISSN: 0278-0046. DOI: 10.1109/TIE.2008.927403.

[6] R. L. Taylor Zienkiewicz O. C. and J.Z. Zhu. *The Finite Element Method: Its Basis and Fundamentals*. Sixth Edition. Butterworth-Heinemann, 2005.

[7] J. Lindström. "Development of an Experimental Permanent-Magnet Motor Drive". PhD thesis. Chalmers University of Technology, 1999.

[8] A.M. El-Refaie et al. "Thermal analysis of multibarrier interior PM synchronous Machine using lumped parameter model". In: *Energy Conversion, IEEE Transactions on* 19.2 (2004), pp. 303 –309. ISSN: 0885-8969. DOI: 10.1109/TEC.2004.827011.

[9] D. Staton, A. Boglietti, and A. Cavagnino. "Solving the more difficult aspects of electric motor thermal analysis". In: *Electric Machines and Drives Conference, 2003. IEMDC'03. IEEE International*. Vol. 2. 2003, 747 –755 vol.2. DOI: 10.1109/IEMDC.2003.1210320.

[10] D. L. Chung. *Applications of Engineering Materials in Structural, Electronics, Thermal, and Other Industries*. CRC Press, 2001. ISBN: 978-1-4200-4097-5.

[11] Cheng S K Cao J C Zhang Y H Li W L Zhang X C. "Thermal Analysis of High Speed Permanent Magnetic Generator". In: *Science China – Technological Sciences* 55.5 (2012), pp. 1419–1426.

[12] J. Saari. "Thermal Analysis of High-Speed Induction Machines". PhD thesis. Acta Polytechnica Scandinavica, 1998.

A   Plots From FEM-simulation

Figures 30 and 31 shows the heat flux and the temperature in the machine according to the FEM simulation.
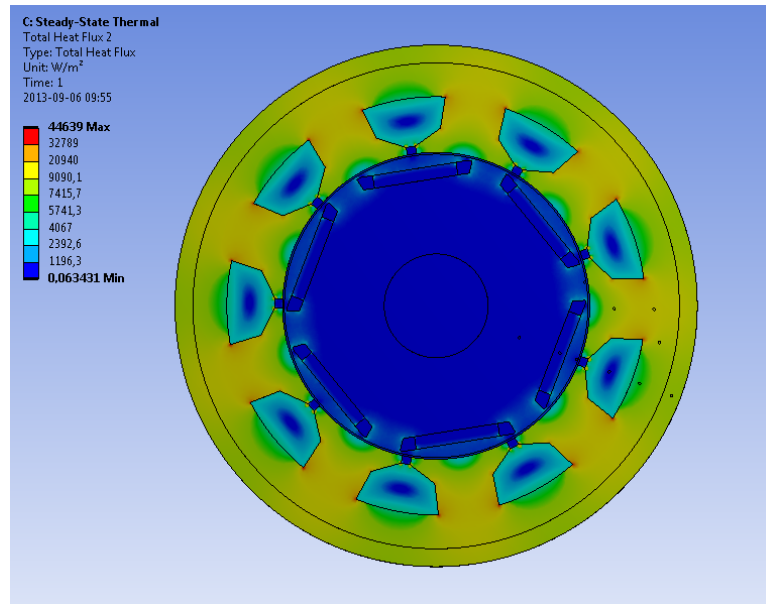

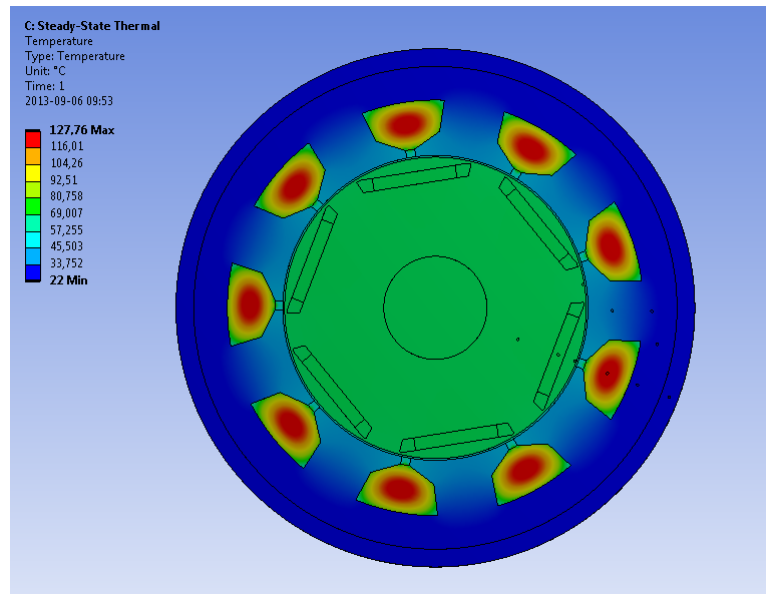Figure 30: The heat flux in the machine at standard settings.

Figure 31: The temperature distribution of the machine at standard settings.

B Detailed Data

Here follows more detailed simulation data as a complement to some of the plots in the thesis.

B.1 Case Study – Node Injection Point

Table 24: Comparison of choice of node locations impact on the thermal network – Stator like object

Node	FEM	Loss in n_{resMid}			Loss in n_{radMid}			Loss in n_{volMid}		
		T	ΔT	$\Delta T[\%]$	T	ΔT	$\Delta T[\%]$	T	ΔT	$\Delta T[\%]$
n_i	79.09	106.90	27.81	35.2	85.26	6.16	7.8	68.26	-10.84	-13.7
n_{resMid}	70.17	106.90	36.74	52.4	85.26	15.09	21.5	68.26	-1.91	-2.7
n_{radMid}	63.45	85.26	21.80	34.4	85.26	21.80	34.4	68.26	4.80	7.6
n_{volMid}	56.13	68.26	12.13	21.6	68.26	12.13	21.6	68.26	12.13	21.6

Table 25: Comparison of choice of node locations impact on the thermal network – Rotor like object

Node	FEM	Loss in n_{resMid}			Loss in n_{radMid}			Loss in n_{volMid}		
		T	ΔT	[%]	T	ΔT	[%]	T	ΔT	[%]
n_i	53.12	58.57	5.45	10.26	54.40	1.28	2.42	50.45	-2.67	-5.03
n_{resMid}	46.55	58.57	12.02	25.83	54.40	7.86	16.88	50.45	3.90	8.38
n_{radMid}	44.82	54.40	9.58	21.38	54.40	9.58	21.38	50.45	5.63	12.55
n_{volMid}	42.96	50.45	7.49	17.43	50.45	7.49	17.43	50.45	7.49	17.43

B.2 Sensitivity Analysis – Node Connections

Table 26 shows the results when changing the values on the connection resistances. From it, a few relations can be pointed out. The first is that that only nodes higher up in the flow path will be affected by a change. Change the air gap, and only the rotor nodes will be affected. Increase the length of the yoke instead, and also the teeth and the slots will grow hotter, all by the same amount.

Secondly, the magnitude of the temperature change caused by a thermal resistance is determined not only by the thermal resistance, but also how large the heat flow is through that connection. According to Table 26 the most significant changes to the magnet node is caused by a change in air gap resistance. Another sensitive connection is the one between the teeth and the yoke, R_{6-7}, where the temperature difference is 16 degrees, and that despite the air gap resistance being almost 30 times higher. The reason for this is that the heat flow from the rotor is only a fraction of the total loss

in the motor which will all pass through the yoke.

Table 26: Sensitivity analysis – Identifying importance of node connections.

Change (%)		Node Temperature [$^{\circ}C$]							
		1.Rotor	2.Magnet	3.Airgap	4.SlotAvg	5.Slot max	6.Tooth	7.Yoke	8.Frame
No Change 66.78		66.77	40.45	104.75	128.47	39.52	26.85	22.2	
R_{1-2}	double	66.78	66.77	40.45	104.75	128.47	39.52	26.85	22.2
R_{1-2}	half	66.78	66.77	40.45	104.75	128.47	39.52	26.85	22.2
R_{2-3}	double	93.1	93.1	40.45	104.75	128.47	39.52	26.85	22.2
R_{2-3}	half	53.61	53.61	40.45	104.75	128.47	39.52	26.85	22.2
R_{3-6}	double	67.62	67.62	41.38	104.75	128.45	39.52	26.85	22.2
R_{3-6}	half	66.35	66.35	39.98	104.75	128.47	39.52	26.85	22.2
R_{4-6}	double	65.41	65.41	38.94	132.59	166.04	38.01	26.85	22.2
R_{4-6}	half	67.94	67.94	41.73	81.05	96.49	40.8	26.85	22.2
R_{4-7}	double	68.19	68.19	42.01	124.92	155.14	41.08	26.85	22.2
R_{4-7}	half	65.18	65.18	38.69	82.05	98.45	37.76	26.85	22.2
R_{6-7}	double	77.59	77.59	52.34	111.99	135.68	51.41	26.85	22.2
R_{6-7}	half	61.13	61.13	34.22	100.96	124.69	33.28	26.85	22.2
R_{7-8}	double	71.0	71.0	45.1	109.4	133.12	44.17	31.5	22.2
R_{7-8}	half	64.67	64.67	38.13	102.43	126.14	37.19	24.52	22.2
R_{8-8}	double	66.96	66.96	40.65	104.95	128.67	39.72	27.05	22.4
R_{8-8}	half	66.68	66.68	40.35	104.65	128.37	39.42	26.75	22.1

C Selected Output From a Simulation

C.1 List of Resistances

The calculated values of the resistances according to the thermal network analysis as presented by generated log file.

```
Resistances:
THERMAL RESISTANCE      VALUE [K/W]
rthShaft                inf
rthRotorMidInner        0.015278
rthRotorMidOuter        0.009882
rthRotorMidOuterFeSeg   0.155214
rthRotorMidOuterMagSeg  0.095945
rthMagnet               0.083088
rthMagnetFe             0.070896
rthRotorOuterSeg        0.002556
rthRotorFeSeg           0.078137
rthRotorMagnetOuterSeg  0.019988
rthAirgap               0.363366
rthToothSeg1            0.013613
rthToothSeg2            0.037519
rthToothSeg3            0.093077
rthToothTot             0.144209
rthToothMidSeg1&2       0.078843
rthToothWing            0.14548
rthSlotOpening          163.2887
rthWindingTot           10.207415
rthYokeInner            0.002284
rthYokeOuter            0.001967
rthYokeTot              0.004252
rthYokeInnerToothSegment 0.048785
rthYokeInnerSlotSegment 0.035532
rthFrame                0.000276
rthRotorOuterPeriph     1.211857
rthToothWingPeriph      0.276938
rthToothMidSeg1&2Periph 0.405174
rthToothSeg3Periph      0.344368
rthToothPeriph          0.253385
rthSlotOpeningPeriph    231.848223
rthYokeInnerPeriph      0.775956
GContactSlot            89.734637
GContactStatorFrame     7787.878788
rthContactStatorFrame   0.001076
GContactMagnets         2519.607843
rthContactMagnet        0.060134
rthSlotTotal            0.995659
rthToothInjectionI      0.050736
rthToothInjectionO      0.092765
```

C.2   List of Connections

Information on the nodes and network connections as presented in the log file.

```
=========================================================================

Solution: Complex Network

=========================================================================


Node temperatures and loss distribution:
#       NODE NAMES          TEMPERATURE       LOSS
1       Rotor               69.84 [C]         0.01    [W]
2       Magnet              70.4 [C]          75.35   [W]
3       RotorOuterFe        69.18 [C]         0.0     [W]
4       RotorOuterMagnet    69.22 [C]         0.0     [W]
5       RotorOuterConnection66.47 [C]         0.0     [W]
6       Airgap              41.83 [C]         90.0    [W]
7       SlotOpening         58.1 [C]          0.0     [W]
8       SlotAverage         107.32 [C]        616.5   [W]
9       SlotMax             131.93 [C]        0.0     [W]
10      ToothWing           42.44 [C]         0.0     [W]
11      Tooth               39.31 [C]         291.62  [W]
12      ToothOuter          40.76 [C]         0.0     [W]
13      YokeInnerSlot       27.46 [C]         0.0     [W]
14      YokeInnerTooth      28.91 [C]         0.0     [W]
15      Yoke                26.85 [C]         386.53  [W]
16      Frame               22.2 [C]          0.0     [W]

        Total Losses:                         1460.01 [W]

   Node Connections:
   NAME       NODE 1              NODE 2              HEATFLOW [P]    THERMAL RESISTANCE [K/W]
   R_{1-1}    Rotor               Ambient             0.0             inf
   R_{1-2}    Rotor               Magnet              -16.99          0.032937
   R_{1-3}    Rotor               RotorOuterFe        17.0            0.038892
   R_{2-4}    Magnet              RotorOuterMagnet    58.36           0.020278
   R_{3-4}    RotorOuterFe        RotorOuterMagnet    -0.37           0.100988
   R_{4-5}    RotorOuterMagnet    RotorOuterConnection58.0           0.047363
   R_{3-5}    RotorOuterFe        RotorOuterConnection17.36          0.156085
   R_{5-6}    RotorOuterConnectionAirgap              75.36           0.32703
   R_{8-9}    SlotAverage         SlotMax             0.0             1000000.0
   R_{6-7}    Airgap              SlotOpening         -1.79           9.071594
   R_{7-8}    SlotOpening         SlotAverage         -4.22           11.656839
   R_{8-13}   SlotAverage         YokeInnerSlot       276.81          0.28852
   R_{8-11}   SlotAverage         Tooth               173.6           0.391762
   R_{8-10}   SlotAverage         ToothWing           161.87          0.400835
   R_{7-10}   SlotOpening         ToothWing           2.43            6.447921
   R_{6-10}   Airgap              ToothWing           -75.8           0.008082
   R_{6-12}   Airgap              ToothOuter          242.95          0.00438
   R_{10-12}  ToothWing           ToothOuter          88.5            0.018948
   R_{12-11}  ToothOuter          Tooth               331.45          0.00438
   R_{11-14}  Tooth               YokeInnerTooth      796.67          0.013052
   R_{13-15}  YokeInnerSlot       Yoke                310.55          0.001974
   R_{14-15}  YokeInnerTooth      Yoke                762.93          0.00271
   R_{14-13}  YokeInnerTooth      YokeInnerSlot       33.75           0.043109
   R_{15-16}  Yoke                Frame               1460.01         0.003181
   R_{16-16}  Frame               Ambient             1460.01         0.000138
```